Piercing the rainbow state: Entanglement on an inhomogeneous spin chain with a defect

Nadir Samos Sáenz de Buruaga,[1] Silvia N. Santalla,[2] Javier Rodríguez-Laguna,[3] and Germán Sierra[1]
[1]*Instituto de Física Teórica UAM/CSIC, Universidad Autónoma de Madrid, Cantoblanco, Madrid, Spain*
[2]*Dto. Física & GISC, Universidad Carlos III de Madrid, Spain*
[3]*Dto. Física Fundamental, Universidad Nacional de Educación a Distancia (UNED), Madrid, Spain*

(Received 7 January 2020; revised manuscript received 21 April 2020; accepted 27 April 2020; published 15 May 2020)

The rainbow state denotes a set of valence bond states organized concentrically around the center of a spin 1/2 chain. It is the ground state of an inhomogeneous XX Hamiltonian and presents a maximal violation of the area law of entanglement entropy. Here, we add a tunable exchange coupling constant at the center, γ, and show that it induces entanglement transitions of the ground state. At very strong inhomogeneity, the rainbow state survives for $0 \leqslant \gamma \leqslant 1$, while outside that region the ground state is a product of dimers. In the weak inhomogeneity regime, the entanglement entropy satisfies a volume law, derived from CFT in curved space-time, with an effective central charge that depends on the inhomogeneity parameter and γ. In all regimes we have found that the entanglement properties are invariant under the transformation $\gamma \longleftrightarrow 1-\gamma$, whose fixed point $\gamma = 1/2$ corresponds to the usual rainbow model. Finally, we study the robustness of nontrivial topological phases in the presence of the defect.

DOI: 10.1103/PhysRevB.101.205121

I. INTRODUCTION

Entanglement provides a very useful connecting thread through condensed matter physics, quantum optics and quantum field theory, towards a unified field of quantum matter [1,2]. One of the most relevant insights is expressed through the area law [3,4]: the entanglement entropy of a block within the ground state (GS) of a local quantum system is, in general terms, proportional to the measure of its boundary [5,6]. Interestingly, the GS of a (1+1)D conformal field is an exception, and the entropy of a block is generically proportional to the logarithm of its volume, with a prefactor which is proportional to the associated central charge [7–10]. There are other interesting exceptions, such as random systems [11–16]. In the strong inhomogeneity limit, the GS of many random systems can be obtained via the Dasgupta-Ma procedure [17,18], which can be engineered to obtain a 1D GS with maximal entanglement between its left and right halves, known as the *rainbow state* [19–22]. This violation of the area law is very robust with respect to the presence of disorder in the hoppings [23,24].

A physical interpretation of the rainbow state can be provided by noticing that the Dirac vacuum on a static (1+1)D metric of optical type can be simulated on a free fermionic lattice with smoothly varying hopping amplitudes [25,26]. Indeed, the hopping amplitudes which characterize the rainbow state can be understood as a (1+1)D anti-de Sitter (AdS) metric [27–30]. Space is exponentially stretched as we move away from the center, giving rise to a similar exponential stretch of the entanglement entropies, transforming the logarithmic law into a volume law. The weak inhomogeneity limit is determined by a deformation of the conformal law and the strong inhomogeneity limit is determined by the Dasgupta-Ma rule, and both fit seamlessly.

Thus it is relevant to ask whether the weak and the strong inhomogeneity limits will match in all possible situations. We have introduced a defect in the center of the rainbow system and considered the entanglement structure as a function of the defect intensity and the curvature. As we will show, both the Dasgupta-Ma and the field theory approach that describes entanglement on a critical chain with a defect [31–34] can be extended to the curved case in the strong and weak inhomogeneity regimes, respectively, providing a complete physical picture.

This paper is organized as follows. Section II discusses our model. The strong inhomogeneity limit, studied with the Dasgupta-Ma RG, is described in detail in Sec. III, while Sec. IV considers the weak-inhomogeneity regime through a perturbation of a conformal field theory. We characterize the entanglement structure via the entropies and the entanglement spectrum, Hamiltonian and contour. A duplication of the defect leads the system to a symmetry protected topological (SPT) phase in coexistence with a trivial dimerized phase, which are discussed in Sec. V. The paper ends with a brief discussion of our conclusions and proposals for further work in Sec. VI.

II. THE MODEL

Let us consider an inhomogeneous XX spin chain with an even number $N = 2L$ whose Hamiltonian is defined as

$$H_L(h,\gamma) = -\frac{1}{2}\sum_{m=-L+1}^{L-1} J_m S^+_{m-1/2} S^-_{m+1/2} + \text{H.c.}, \qquad (1)$$

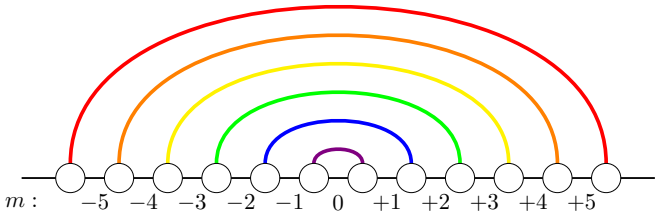

FIG. 1. Illustrating the rainbow state, GS of $H_L(h, 1/2)$ with $L = 6$, for $h \gg 1$. Links are indexed by the integer m. The bonds are established between sites n and $-n$ for $n \in \{\pm 1/2, \ldots, \pm(L - 1/2)\}$.

and by performing a Jordan-Wigner transformation, its fermionic version:

$$H_L(h, \gamma) = -\frac{1}{2} \sum_{m=-L+1}^{L-1} J_m c^\dagger_{m-1/2} c_{m+1/2} + \text{H.c.}, \tag{2}$$

where $c_n(c^\dagger_n)$, with $n = \pm\frac{1}{2}, \pm\frac{3}{2} \cdots \pm (L - \frac{1}{2})$ are fermionic annihilation (creation) operators that obey the standard anticommutation relations. The hopping parameters J_m are

$$J_m = \begin{cases} e^{-h|m|} & \text{if } m \neq 0, \\ e^{-h\gamma} & m = 0, \end{cases} \tag{3}$$

where $h \geqslant 0$ is the inhomogeneity parameter, and $\gamma \in \mathbb{R}$ parametrizes the value of the central hopping that we shall interpret as a defect. Notice that sites have half-integer indices, while links have integer ones. The Hamiltonian presents spatial inversion symmetry around the central bond: $J_m = J_{-m}$, which we will label bond-centered symmetry (bcs) [22].

For $\gamma = 1/2$, we recover the so-called rainbow Hamiltonian, whose ground state is the rainbow state [19–21]. In the strong-coupling regime ($h \gg 1$), the GS of $H_L(h, 1/2)$ is a valence bond solid (VBS) made of bonds connecting opposite sites of the chain, as is illustrated in Fig. 1. On the other hand, the weak inhomogeneity limit ($h \ll 1$) is characterized by the free-fermion conformal field theory (CFT) on a different space-time, provided by the metric

$$ds^2 = -e^{-2h|x|} dt^2 + dx^2, \tag{4}$$

thus justifying our claim that the rainbow state, in the weak inhomogeneity regime, corresponds to the anti de Sitter (AdS) Dirac vacuum. Using CFT tools, it has been proved that the GS of Hamiltonian $H_L(h, 1/2)$ presents linear entanglement for all h, with an entropy per site $S/N \approx h/6$ (von Neumann entanglement entropy) [27,28]. We will discuss some of these properties in detail in the corresponding sections, when considering how they are modified by the defect.

III. THE STRONG INHOMOGENEITY LIMIT

When the inhomogeneity is large enough, it can be addressed through renormalization group (RG) schemes. In particular, we will use the Dasgupta-Ma procedure, also known as strong-disorder renormalization group (SDRG) [17], that was originally created to characterize random spin chains, but can be immediately extended to fermionic chains via de Jordan-Wigner transformation [15]. At each step of the RG, four spins are considered: the two spins s_i and s_{i+1} linked by the strongest coupling (highest absolute value of J_i) and their nearest neighbors, s_{i-1} and s_{i+2}. The two spins coupled by J_i are integrated out by forming a valence bond state (VBS) and the two remaining ones are coupled with a new effective coupling constant that is obtained by means of second-order perturbation theory. For a free-fermionic chain with a Hamiltonian such as (2), the effective coupling takes the expression

$$\tilde{J}_i = -\frac{J_{i-1} J_{i+1}}{J_i}, \quad |J_i| \gg |J_{i\pm1}|. \tag{5}$$

The GS predicted by the SDRG is a valence-bond solid (VBS), i.e., a tensor product of bonds:

$$|\text{GS}\rangle = \prod_{k=1}^{L} \left(b^{\eta_k}_{i_k, j_k}\right)^\dagger |0\rangle, \tag{6}$$

where $\eta_k = \pm 1$ is a phase given by Eq. (5), $|0\rangle$ is the Fock vacuum, and $b^+_{i,j}$ ($b^-_{i,j}$) are bonding (antibonding) operators that create a fermionic excitation joining sites i and j.

$$(b^\pm_{ij})^\dagger = \frac{1}{\sqrt{2}} (c^\dagger_i \pm c^\dagger_j). \tag{7}$$

They satisfy usual canonical anticommutation relations.

Let us consider the GS of Hamiltonian (2) under the light of the SDRG for $h \gg 1$. For simplicity, we will only consider even L (the case of odd L can be straightforwardly obtained), as a function of the defect parameter γ. The different phases will be discussed along the panels of Fig. 2.

The different ground states obtained by means of the SDRG are presented in Table I, please refer to Appendix A for the details. All of them are obtained at half filling and it is important to note that the validity of the SDRG improves when the renormalized hopping is much stronger than the surrounding ones, so all the GS that we have found are better approximations for bigger h (and eventually they are exact for $h \to \infty$ as they are fixed points of the RG).

We obtain a rainbow phase whose GS is constituted by concentric bonds, two dimerized phases that are related to the two phases of the Su-Schrieffer-Heeger (SSH) model [35,36] and two transition phases whose structure is a blend of the two previous ones and it shall be understood in what follows.

It is worth noticing the existence of a symmetry between the cases $\gamma \leqslant 0$ and $\gamma \geqslant 1$. Consider a system $H_L(h, \gamma < 1)$. After performing the first RG step, the new system is described by the renormalized Hamiltonian $H_{L-1}(h, 2 - \gamma)$. If we now subtract one from all the log-hoppings (or equivalently we divide by e^{-h} all the hoppings) the Hamiltonian becomes $e^h H_{L-1}(h, 1 - \gamma)$, which describes a system of $N - 2$ sites and a defect with strength $1 - \gamma$. Hence, the transformation

$$\gamma \to \tilde{\gamma} = 1 - \gamma, \tag{8}$$

leaves the structure invariant up to a global constant. Note that this symmetry can be considered as a local strong-weak duality of the defects, leaving the $\gamma = 1/2$ point invariant.

The aforementioned description, along with the evidences obtained by the study of the energies, the correlators and the

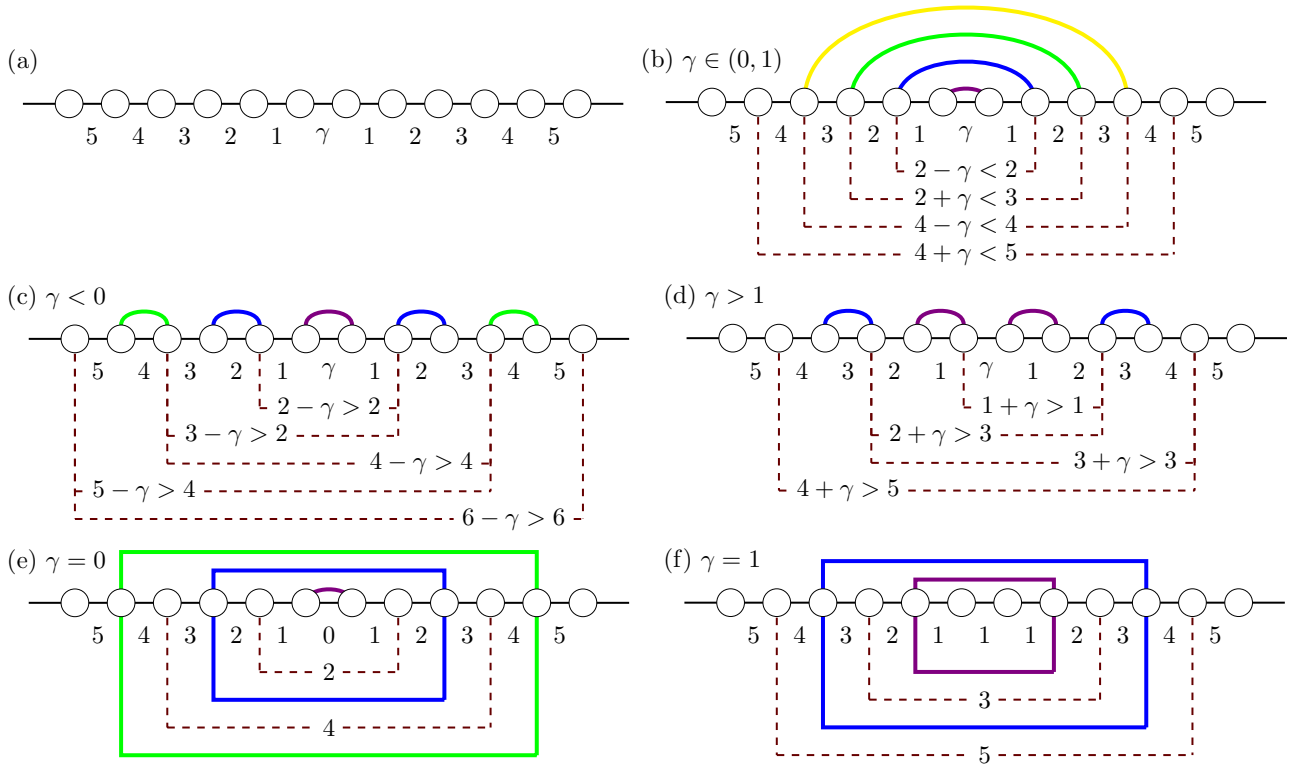

FIG. 2. (a) Illustration of the rainbow chain with a central defect, showing the log-couplings on each link (see Appendix A); (b) SDRG procedure in the $\gamma \in (0, 1)$ case, leading to the rainbow phase; (c) SDRG for the $\gamma < 0$ case; (d) SDRG for the $\gamma > 1$ case, both leading to dimerized phases; (e) and (f) transition cases, where the SDRG approximation is not valid; the dashed boxes mark the ties between the couplings, which demand a different RG approach.

entanglement entropy, allow us to claim that the rainbow system with a defect presents two entanglement transitions [37] in the strong inhomogeneity regime.

A. Energies

Let us consider the single-body energy levels $E_k(h, \gamma)$ ($k \in \{0, \ldots, N-1\}$) of $H_L(h, \gamma)$, obtained by diagonalizing the corresponding hopping matrix. Due to the particle-hole symmetry, $E_k = -E_{N-k}$, we need only consider values up to $L-1$. For large h, these single-body energy levels correspond to the couplings associated with each valence bond, thus leading us to propose that the following limits are finite,

$$\lim_{h\to\infty} -\frac{\ln|E_k(h,\gamma)|}{h} = \Xi_k(\gamma). \tag{9}$$

Figure 3 (top) plots these values, $\Xi_k(\gamma)$ as a function of γ for $L = 12$, obtained numerically using $h = 15$ (for which convergence has been achieved). Notice the

TABLE I. All the possible ground states obtained via the SDRG in terms of the defect amplitude γ.

Phase	Figure 2	Ground state $\|GS\rangle$
Rainbow phase $\gamma \in (0, 1)$	(b)	$\prod_{i=0}^{L-1} \left(b^{\eta_i}_{-i-1/2,i+1/2}\right)^\dagger \|0\rangle, \quad \eta_i = (-1)^i$
Dimerized phase I $\gamma < 0$	(c)	$(b^-_{-L+\frac{1}{2},L-\frac{1}{2}})^\dagger \prod_{i=-\frac{L}{2}+1}^{\frac{L}{2}-1} (b^+_{2i-\frac{1}{2},2i+\frac{1}{2}})^\dagger \|0\rangle$
Dimerized phase II $\gamma > 1$	(d)	$\prod_{i=-\frac{L-1}{2}}^{\frac{L-1}{2}} (b^+_{2i-\frac{1}{2},2i+\frac{1}{2}})^\dagger \|0\rangle$
Transition phase I $\gamma = 0$	(e)	$(b^-_{-L+\frac{1}{2},L-\frac{1}{2}})^\dagger \prod_{i=1}^{\frac{L}{4}} \left(d^{\eta_i}_{2i+\frac{1}{2}}\right)^\dagger (b^+_{-\frac{1}{2},\frac{1}{2}})^\dagger \|0\rangle,$
Transition phase II $\gamma = 1$	(f)	$\prod_{i=1}^{\frac{L}{2}} \left(d^{\eta_i}_{2i-\frac{1}{2}}\right)^\dagger \|0\rangle$

where $d^\pm_k$ are operators that create two particles on four fermionic sites (see Appendix C),

$$\left(d_i^{\eta_i}\right)^\dagger = (v^{\eta_i})^\dagger \left(u^{\eta_{i-1}}\right)^\dagger |0\rangle, \quad \eta_i = (-1)^i,$$
$$u_i^\pm = \tfrac{1}{\sqrt{5+\sqrt{5}}}(c_{-i} \pm c_i) + \tfrac{1}{\sqrt{5-\sqrt{5}}}(c_{-i+1} \pm c_{i-1}),$$
$$v_i^\pm = \tfrac{1}{\sqrt{5-\sqrt{5}}}(c_{-i} \pm c_i) + \tfrac{1}{\sqrt{5+\sqrt{5}}}(c_{-i+1} \pm c_{i-1}).$$

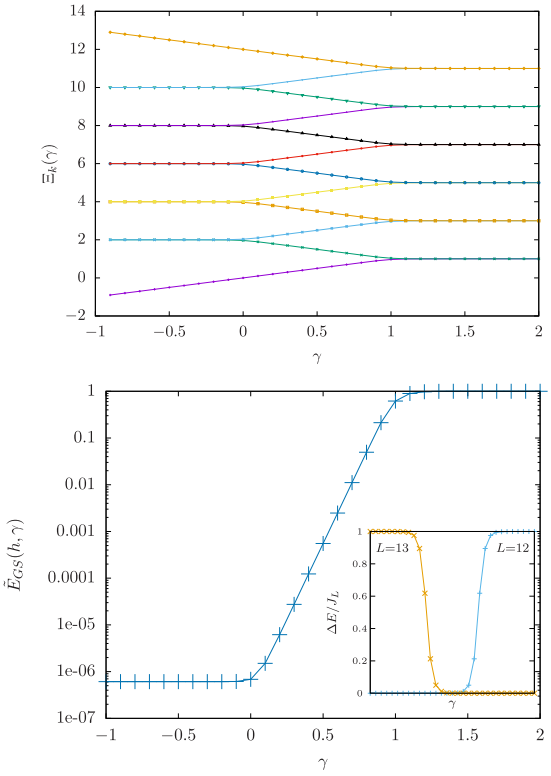

FIG. 3. (Top) Plot of $\Xi_k(\gamma)$, obtained numerically for $L = 12$ and $h = 15$, see Eq. (9). Each curve matches the renormalized log-couplings along the SDRG procedure. (Bottom) Ground state energy, with the lowest single-body energy level removed, as a function of γ for the same system. (Inset) Energy gap in units of the lowest energy scale of the system, $\Delta E/J_L$, for $L = 12$ and $L = 13$.

clear pattern: for $\gamma > 1$, all energy levels are degenerate, $\Xi_{2k}(\gamma) = \Xi_{2k+1}(\gamma) = 2k + 1 \quad \text{for} \quad k \in \{0, \ldots, L/2 - 1\}$, while for $\gamma < 0$ all energy levels are degenerate and constant, except the first and last which vary exponentially with γ, $\Xi_{2k-1}(\gamma) = \Xi_{2k}(\gamma) = 2k$ for $k \in \{1, \ldots, L/2 - 1\}$. Indeed, these values correspond to the energies associated to the successive valence bonds of the dimerized phases. On the other hand, for $\gamma \in (0, 1)$ the energy levels are not degenerate, and we can observe the same alternation of the renormalized log-couplings that we observed in the SDRG description: $\Xi_k(\gamma) = k + 1/2 + (-1)^k(\gamma - 1/2)$. Thus the transition points, $\gamma = 0$ and $\gamma = 1$, correspond to the points where the degeneracy starts and ends.

The ground state energy is the sum of the energies of the occupied orbitals, $E_{\mathrm{GS}}(h, \gamma) = \sum_{k=0}^{L-1} E_k(h, \gamma)$. Notice that for large h and $\gamma > 1$, the lowest single-body energy $E_0(h, \gamma)$ is the main contribution to $E_{\mathrm{GS}}(h, \gamma)$ as its value grows exponentially with γ (see the lowest line of the top panel of Fig. 3), so we have considered instead the quantity

$$\tilde{E}_{\mathrm{GS}}(h, \gamma) = -E_{\mathrm{GS}}(h, \gamma) + E_0(h, \gamma) = -\sum_{k=1}^{L-1} E_k(h, \gamma). \tag{10}$$

The values of $\tilde{E}_{\mathrm{GS}}(h, \gamma)$ are plotted in Fig. 3 (bottom) for the same system $L = 12$ and $h = 15$ in logarithmic scale. Notice

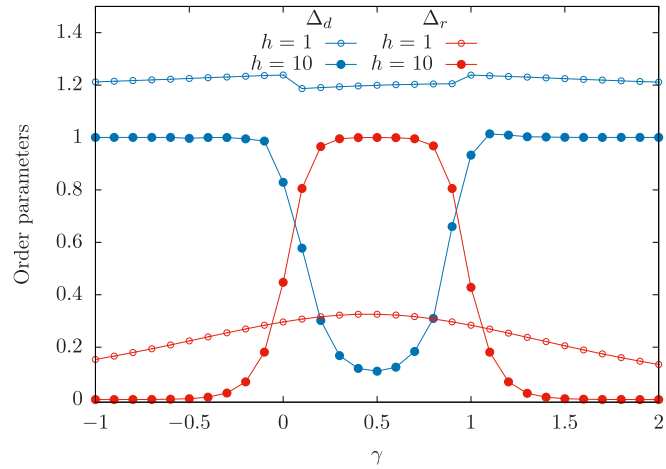

FIG. 4. Dimerization parameter Δ_d (blue curves) and rainbow parameter Δ_r (red curves) as a function of γ, for a system of $L = 10$. As the inhomogeneity parameter h grows, Δ_d approaches one in the dimerized phases and zero in the rainbow phase, while Δ_r approaches one in the rainbow phase and zero in the dimerized phases.

the three regions: for the dimerized phases, $\tilde{E}_{\mathrm{GS}}(h, \gamma)$ stays constant, while for the rainbow phase it grows exponentially. Indeed, for $h \to \infty$, the energy curve $\ln(\tilde{E}_{\mathrm{GS}}(h, \gamma))/h$ becomes nonsmooth at $\gamma = 0$ and $\gamma = 1$, pointing at a phase transition.

In addition, the inset of Fig. 3 (bottom) plots the energy gap $\Delta E/J_L = (E_L - E_{L-1})/J_L$, normalized with the lowest energy scale of the system (the lowest coupling constant). We can see that it presents two types of behaviors, depending whether the spectrum has a long range mode [with $E_{L-1}(h, \gamma) = e^{-Lh}$]: for even L it is close to zero ($\Delta E/J_L \sim e^{-h}$) for $\gamma < 1$, while for odd L it is close to zero ($\Delta E/J_L \sim e^{-h}$) for $\gamma > 0$. For $\gamma \in [0, 1]$, it is close to zero for all sizes.

B. Correlations and order parameters

In order to provide further support to our idea that there is a phase transition at $\gamma = 0$ and $\gamma = 1$ in the strong inhomogeneity limit, let us provide two order parameters that we will call the dimerization parameter Δ_d and the rainbow parameter Δ_r,

$$\Delta_d = \frac{1}{N} \sum_{i=-L+\frac{1}{2}}^{L-\frac{1}{2}} |\langle\psi|c_i^\dagger c_{i+1}|\psi\rangle|, \tag{11}$$

$$\Delta_r = \frac{1}{L} \sum_{i=-\frac{1}{2}}^{L-\frac{1}{2}} |\langle\psi|c_i^\dagger c_{-i}|\psi\rangle|. \tag{12}$$

Figure 4 shows the behavior of these two order parameters as a function of γ, for two values of h and $L = 10$. For large h ($h = 10$ in the figure), we see that the rainbow parameter Δ_r tends to 1 in the rainbow phase [$\gamma \in (0, 1)$], while it decays to zero in the dimerized phases. The opposite behavior is true for the dimerization parameter Δ_d.

C. Entanglement entropy

Given a system in a pure state, $|\psi\rangle$, the entanglement entropy (EE) of a block A is defined as the von Neumann entropy of its associated reduced density matrix $\rho_A = \mathrm{Tr}\bar{A}|\psi\rangle\langle\psi|$, where $\bar{A}$ is the complementary of A.

$$S[\rho_A] = -\mathrm{Tr}_A \ln(\rho_A), \tag{13}$$

while the Rényi entropy of order n is defined as

$$S^{(n)}[\rho_A] = \frac{1}{1-n} \ln \mathrm{Tr}_A^n. \tag{14}$$

Needless to say, the different entanglement entropies are determined by the eigenvalues of the reduced density matrix, also known as entanglement spectrum (ES). There is well known procedure [38] in order to obtain the ES through the spectrum of the correlation matrix restricted to the block, $\langle c_i^\dagger c_j\rangle$, with $i, j \in A$. The correlation matrices can be exactly obtained in the strong inhomogeneity limit, as it is shown in Appendix D. On the other hand, when the state is a VBS, we can evaluate the EE just by counting the number of bonds which are broken when we detach the block from its environment, and multiplying by ln(2), and the same is true for all Rényi entropies.

We have considered two different types of blocks: lateral blocks start from the extreme of the chain, while central blocks are symmetric with respect to the center. In the next paragraphs we will describe the behavior of their entanglement.

1. Lateral blocks. Half chain entropies

Lateral blocks $A_\ell = \{-L+\frac{1}{2}, \ldots, -L+\frac{1}{2}+\ell\}$ are contiguous blocks containing one of the extremes of the chain. Concretely, we will be interested in the EE of the half chain, $S(L) = S[A_L]$ in the strong inhomogeneity regime for different values of γ. Let us remind the reader that we will only consider even L for simplicity, and that the different phases can be visualized either in Figs. 2 and 6, where the blocks contain ℓ sites from the upper leg, starting from the right end.

(1) Rainbow phase, $\gamma \in (0, 1)$. The EE (and all other Rényi entropies) are merely proportional to the length up to $\ell = L$, $S[A_\ell]_{\gamma\in(0,1)} = \ln(2)\min(\ell, 2L+1-\ell)$.

(2) Dimerized phases, $\gamma < 0$ or $\gamma > 1$. The lateral blocks cut either zero or one bonds for $\gamma > 1$, $S[A_\ell]_{\gamma>1} = \ln(2)(1-(-1)^\ell)/2$; yet, for $\gamma < 0$ there is always a long-distance bond joining both ends, thus $S[A_\ell]_{\gamma<0} = \ln(2)(1+(1+(-1)^\ell)/2)$.

(3) Transition cases, $\gamma = 0$ and 1. The state is not a VBS, so the EE of a block can not be evaluated just by counting broken bonds. As we can see in the folded view, Fig. 6, the sites are grouped into plaquettes (except, maybe, for the extremes and the central link). Cutting one of these plaquettes horizontally in half contributes a finite amount of entanglement S_a, which is exactly evaluated in Appendix D [see Eq. (8)]:

$$S_a = \ln 20 - \frac{4\tanh^{-1}\left(\frac{2}{\sqrt{5}}\right)}{\sqrt{5}} \approx 0.4133, \tag{15}$$

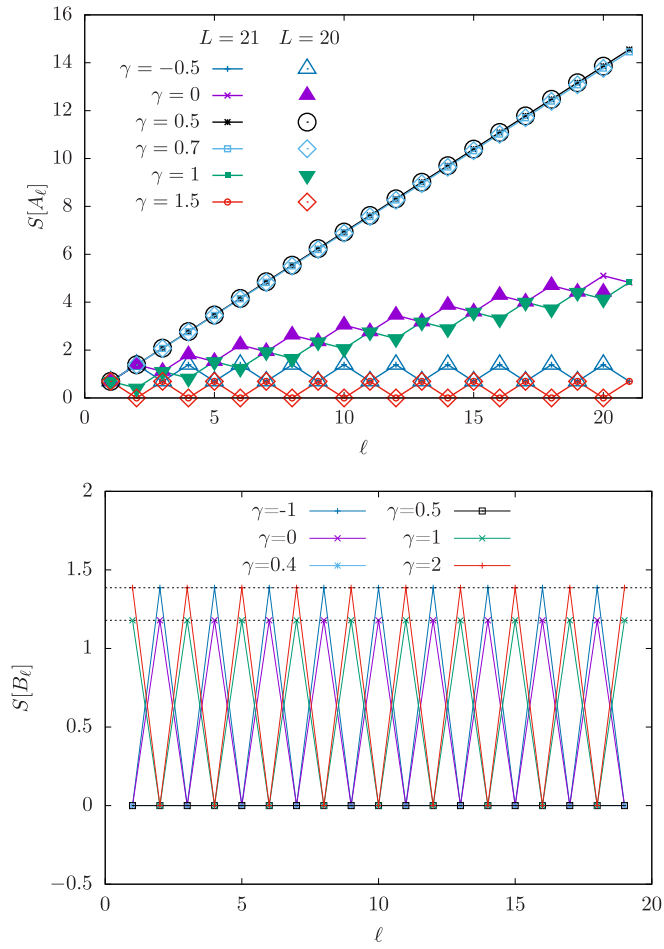

FIG. 5. (Top) Entanglement entropy of blocks of size ℓ using $h = 10$ for two systems, of size $L = 20$ and 21, for different values of γ. (Bottom) EE of the central blocks B_ℓ for $L = 20$ sites and $h = 10$. The top horizontal line marks $2\ln 2$, and the lower one marks S_b, see Eq. (16)

we are thus led to exact expressions for the half-chain entropy: $S[A_L]_{\gamma=1} = S_a\, L/2$ ln(2), $S[A_L]_{\gamma=0} = S_a\,(L/2-1) + 2\ln(2)$.

All these results can be checked in Fig. 5 (top) for two rainbow chains with $L = 20$ and 21, using $h = 10$, where $S[A_\ell]$ is plotted as a function of ℓ for different values of γ. We can see that the $\gamma = -0.5$ and 1.5 cases show a properly dimerized behavior, and the $\gamma = 0.5$ values correspond to the rainbow, linear with (maximal) slope ln(2). For the transition points $\gamma = 0$ and 1, we can observe a linear behavior (with parity oscillations) with a slope S_a.

2. Central blocks

The structure of the different phases can be properly understood if we fold the chain around the central link, as it is shown in Fig. 6(a), converting the chain into a two-rung ladder where sites $+k$ and $-k$ face each other [22]. This transformation converts rainbow bonds into vertical bonds and the remaining local bonds into horizontal bonds. The lower panels of Fig. 6 present the bond structure as a function of γ.

In this section, we consider the EE of central blocks, symmetrically placed around the center of the chain,

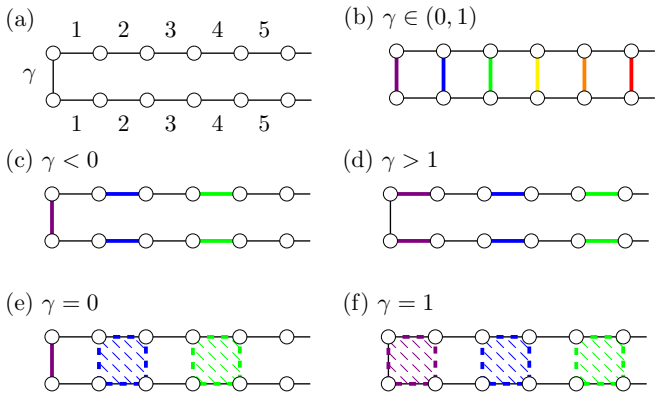

FIG. 6. (a) Folding the rainbow into a two-rung ladder; (b) folded rainbow structure, obtained for $\gamma \in (0, 1)$; [(c) and (d)] folded dimerized structures, for $\gamma < 0$ and $\gamma > 1$; [(e) and (f)] folded versions of the transition points, with the plaquettes marked where operators $d^\dagger$ act, see Eq. (8).

$B_\ell = \{-\ell + \frac{1}{2}, \cdots, \ell - \frac{1}{2}\}$. See Fig. 6, where the blocks now include ℓ rungs starting from the left extreme.

(1) Rainbow phase, $\gamma \in (0, 1)$: we always have $S[B_\ell]_{\gamma\in(0,1)} = 0$.

(2) Dimerized phases, $\gamma < 0$ or $\gamma > 1$: central blocks either cut zero or two bonds. Always usign even L we have $S[B_\ell]_{\gamma<0} = (1 + (-1)^\ell)\ln(2)$ and $S[B_\ell]_{\gamma>1} = (1 - (-1)^\ell)\ln(2)$.

(3) Transition phases, $\gamma = 0$ or $\gamma = 1$: central blocks can cut plaquettes in half vertically, in the folded view. Each such cut contributes a finite amount of entanglement, given by [see Appendix D and Eq. (8)]:

$$S_b = \ln 5 - \frac{\coth^{-1}(\sqrt{5})}{\sqrt{5}} \approx 1.1790, \tag{16}$$

which leads us to the expressions $S[B_\ell]_{\gamma=0} = (1 + (-1)^\ell)S_b$ and $S[B_\ell]_{\gamma=1} = (1 - (-1)^\ell)S_b$.

All these features can be checked in Fig. 5 (bottom), where we can see the central blocks entropy $S[B_\ell]$ as a function of ℓ for different values of γ. Note that the EE of the central blocks is always bounded, thus obeying the area law. Nonlocal fermionic excitations of the type $b_{i,-i}$ and d_i [see Eqs. (7) and (8)] are made local by the folding operation previously discussed [22], and allows to describe the system state using only short range entanglement.

It is important to realize that it is possible to find local blocks whose EE is zero for all the defect amplitudes (see Fig. 6). In the previous work [22], it is shown that the bcs system belongs to a trivial topological phase, as the GS can be written as a MPS with bond dimension 1 and the EE of the central blocks is zero. Here we see that the local defect does not modify this property, meaning that the bcs system with local defect γ is also in the trivial phase. This is expected, as a local perturbation cannot change the topology of the system. On Sec. V, we will discuss the site centered symmetry case, that presents interesting topological features.

IV. WEAK INHOMOGENEITY: DEFECT ON A DEFORMED BACKGROUND

It is relevant to ask whether the phases described in the strong inhomogeneity limit and the corresponding entanglement transitions extend into the weak inhomogeneity regime. The answer is no, but some relevant traits do.

In Fig. 7, we show the dependence on h of the EE of the half chain, $S(L) = S[A_L]$, for different values of γ. We can observe a perfect symmetry between γ and $1 - \gamma$, and the three different trends in the large h limit that we have explained on the previous section: for $\gamma \in (0, 1)$ the EE reaches its maximal value; for $\gamma \in \{0, 1\}$, it reaches an intermediate value ($S_a L/2$); for $\gamma \notin [0, 1]$, it stays at $\ln(2)$. Interestingly, the behavior is remarkably different for lower values of h, as we will discuss.

For $h = 0$, the Hamiltonian (2) becomes the standard massless free-fermionic chain with open boundary conditions which can be described at low energies by a conformal field theory (CFT) with $c = 1$. It is interesting to discuss first such a system in presence of a defect.

A. Homogeneous chain with defect

Let us consider an open homogeneous free fermionic chain and a defect on its central link, parametrized by a coupling parameter τ,

$$H_\tau = -\frac{\tau}{2} c^\dagger_{-\frac{1}{2}} c_{\frac{1}{2}} - \frac{1}{2} \sum_{n=1/2}^{L-3/2} c^\dagger_n c_{n+1} + c^\dagger_{-n} c_{-n-1} + \text{H.c.} \tag{17}$$

Let us take the continuum limit of (17) and characterize its low-energy properties by expanding the local operators c_n into slow left/right moving components $\psi_{\{L,R\}}$ around the Fermi points, and introducing a physical coordinate $x = an$, with lattice constant $a \to 0$, while $L \to \infty$ with $\mathcal{L} = aL$ fixed.

$$c_m \approx \sqrt{a}(e^{ik_F x}\psi_L(x) + e^{-ik_F x}\psi_R(x)). \tag{18}$$

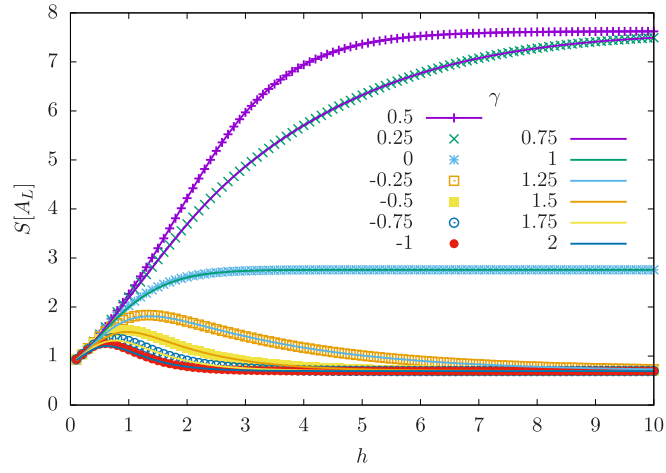

FIG. 7. EE of the half system $N = 22$ as a function of h for different values of the defect strength γ.

The boundary conditions satisfied by the fields at the edge boundaries $\psi_{L,R}(\pm\mathcal{L})$ are obtained by imposing $c_{\pm(L+\frac{1}{2})}=0$:

$$\psi_L(\pm\mathcal{L}) = e^{i\pi(L\pm\frac{1}{2})}\psi_R(\pm\mathcal{L}). \tag{19}$$

In order to characterize the effect of the defect τ, we need to distinguish between the fields on the left side $\psi^I_{L,R}$ and the right side $\psi^{II}_{L,R}$ of the defect, which are related by a transfer matrix $\psi^I = T\psi^{II}$ (see Appendix E):

$$\begin{pmatrix}\psi^I_L\\ \psi^I_R\end{pmatrix} = \frac{1}{2\tau}\begin{pmatrix}\tau^2+1 & -i(\tau^2-1)\\ i(\tau^2-1) & \tau^2+1\end{pmatrix}\begin{pmatrix}\psi^{II}_L\\ \psi^{II}_R\end{pmatrix}. \tag{20}$$

It is important to realize that T only depends on the defect and a vicinity of radius a (lattice sites $\pm\frac{1}{2}$ and $\pm\frac{3}{2}$). Also notice that for $\tau=1$, $T=\mathbb{I}$. Following Ref. [39], we can associate this transfer matrix to the one associated with a massless Dirac fermion with a δ term associated to a mass m and to a chiral mass m',

$$T_D = \frac{1}{1-r^2-r'^2}\begin{pmatrix}1+r^2+r'^2 & 2(ir+r')\\ 2(-ir+r') & 1+r^2+r'^2\end{pmatrix}, \tag{21}$$

where $r\propto m$ and $r'\propto m'$ are the reflection coefficients associated to both terms. If we assume $r'=0$ and compare with Eq. (20) we find that

$$r = \frac{1-\tau}{\tau+1}. \tag{22}$$

Hence, the field theory associated to the homogeneous system in presence of a defect Eq. (17) is a massless Dirac fermion with a δ potential term that mixes the left and right moving fermions generating a local mass placed at the center.

The entanglement properties of this system were studied by Eisler and Peschel [34]. The authors used a conformal mapping to the isotropic $2D$ Ising model to show that the EE of the half chain presents a logarithmic behavior, as predicted by CFT, but with a coefficient that depends on the strength of the defect which they called effective central charge:

$$S(L) = \frac{c_{\text{eff}}}{6}\ln L + c', \tag{23}$$

with

$$c_{\text{eff}} = \frac{6}{\pi^2}I(s), \tag{24}$$

and $I(s)$ given by (see Eq. (26) of Ref. [34]):

$$\begin{aligned}I(s) = -\tfrac{1}{2}[&((1+s)\ln(1+s)+(1-s)\ln(1-s))\ln s\\ &+(1+s)\text{Li}_2(-s)+(1-s)\text{Li}_2(s)],\end{aligned}$$

with $s=\sin(2\arctan\tau)$ and $\text{Li}_2(z)$ is the dilogarithm function [40].

B. Field theory of the rainbow model with a defect

Let us return to our rainbow model with a defect. In order to build the field theory describing the low-energy physics of Hamiltonian (2) in the weak inhomogeneity regime we need to obtain the transfer matrix $T_{h,\gamma}$ associated to the defect. Since the defect is local, we will conjecture that $T_{h,\gamma}$ is determined by the defect and its closest vicinity (see Appendix E):

$$T_{h,\gamma} = \frac{1}{2}e^{h(\gamma-\frac{1}{2})}\begin{pmatrix}e^{-2h(\gamma-\frac{1}{2})}+1 & -i(e^{-2h(\gamma-\frac{1}{2})}-1)\\ i(e^{-2h(\gamma-\frac{1}{2})}-1) & e^{-2h(\gamma-\frac{1}{2})}+1\end{pmatrix}. \tag{25}$$

Note that $T_{h,\gamma}=T$ described in Eq. (20) if we define

$$\tau = e^{-h(\gamma-1/2)}. \tag{26}$$

Notice that the symmetry $\gamma\to 1-\gamma$ described in the previous section is also present in the transfer matrix: $T_{h,1-\gamma}$ is $T_{h,\gamma}$ with opposite signs in the non diagonal terms and that $\tau=1$ if $h=0$ but also if $\gamma=\frac{1}{2}$. This implies that the defect has no effect in $H_L(h,\frac{1}{2})$ or, in other terms, we will say that the defect is absent. Indeed, evaluating the continuum limit of Eq. (18) over Eq. (2) leads to an effective Hamiltonian [21,27,28]:

$$H \approx i\int_{-\tilde{L}}^{\tilde{L}} d\tilde{x}[\tilde{\psi}^\dagger_L\partial_{\tilde{x}}\tilde{\psi}_L - \tilde{\psi}^\dagger_R\partial_{\tilde{x}}\tilde{\psi}_R], \tag{27}$$

where $\tilde{x}$ is given by

$$\tilde{x} \equiv \text{sign}(x)\frac{e^{h|x|}-1}{h} \tag{28}$$

and

$$\tilde{\psi}_{\{L,R\}}(\tilde{x}) = \left(\frac{dx}{d\tilde{x}}\right)^{1/2}\psi_{\{L,R\}}(x). \tag{29}$$

Thus our field theory is the free Dirac field on a background metric given by

$$ds^2 = -e^{-2h|x|}dt^2 + dx^2, \tag{30}$$

i.e., a static metric, defined by a local speed of light or local Fermi velocity $v_F(x)=e^{-h|x|}$.

The metric (30) is Weyl equivalent to the flat metric with the Weyl factor $e^{-h|x|}$, equal to the continuum limit of the hopping amplitudes Eq. (3). Moreover, the metric has a scalar curvature given by $R(x)=2h\delta(x)-h^2$, i.e., except at the origin, it is an homogeneous manifold with negative curvature that can be mapped to the Poincaré metric in the upper half-plane [26] or the anti-de Sitter (AdS) metric in 1+1D [29]. As a consequence, the field theory associated to the Hamiltonian $H_L(h,\gamma\neq\frac{1}{2})$ for low energies should be described by a free Dirac theory with a local defect—which is analogous to the one studied in the previous section—but in the background metric described above. In what follows, we show that this is the case by studying the entanglement properties such as the entanglement entropy, the entanglement spectrum, the entanglement Hamiltonian and the entanglement contour.

C. Entanglement entropy

In the case of absence of defect, $\gamma=\frac{1}{2}$, the EE can be evaluated for intervals of the form $(-L,x)$ within a 2D CFT [7–10], leading to the expression

$$S^{(n)}_{\text{CFT}}(x) = c\frac{n+1}{12n}\ln Y(x), \tag{31}$$

where

$$Y(x) = \frac{2L}{\pi\epsilon}\sin\left(\frac{\pi(L+x)}{2L}\right), \tag{32}$$

and ϵ is the UV cutoff. However, the actual entropy of the discrete state is not exactly equal to that because a nonuniversal term must be added. Its value is exactly known in the case of the free-fermionic field [14,41] and will not be considered here. We can compute the universal part of the EE by making an appropriate use of transformation (28) on expression (31). Indeed, besides the transformation of L and x, we need to take into account the transformation of the UV cutoff ϵ, through the Weyl factor, $\tilde{\epsilon} = e^{h|x|}\,\epsilon$ in our metric. We obtain

$$S^{(n)}_{\gamma=\frac{1}{2}}(x) = c\frac{n+1}{12n}\ln\tilde{Y}(x), \tag{33}$$

with

$$\tilde{Y}(x) = e^{-h|x|}\frac{e^{hL}-1}{\pi h}\cos\left(\frac{\pi}{2}\frac{e^{h|x|}-1}{e^{hL}-1}\right). \tag{34}$$

The half chain EE scales linearly:

$$S_{\gamma=\frac{1}{2}}(L) \approx \frac{c\,hL}{6}. \tag{35}$$

However, the defect ($\gamma \neq \frac{1}{2}$) creates a mass and introduces a scale, breaking the conformal invariance of the system. As a consequence, the previous formulas can not be applied to compute the EE. Nevertheless, the EE should follow Eq. (24), with the modifications associated to the change of background. Indeed, we should modify Eq. (35) as

$$S_\gamma(L) \approx \frac{c_{\text{eff}}(\tau)\,hL}{6}. \tag{36}$$

where τ is given by Eq. (26). In order to check this, we have obtained the entropy per site, defined for convenience as

$$s(h,\gamma) = \lim_{L\to\infty}\frac{6S[A_L]}{L}. \tag{37}$$

The values of $s(h,\gamma)$ are obtained through a linear fit. Figure 8 (top) shows this entropy per site as a function of h for several values of γ. For very low values of h, all curves seem to collapse. Yet, for $\gamma \notin [0,1]$, the curve $s(h)$ eventually presents a maximum and decays to zero. This is a signature that the system will obey the area law in the strong inhomogeneity limit. The validity of Eq. (36) can be checked with the soft continuous lines, which correspond to the theoretical prediction. Indeed, for low values of h the prediction is very accurate, losing this accuracy for large inhomogeneity ($h \approx 1.5$).

Furthermore, Eq. (36) suggests that the entropy per site will collapse if we plot $s(h,\gamma)/h$ as a function of a measure of the defect intensity, $h(\gamma - 1/2)$. Indeed, this collapse can be seen in the bottom panel of Fig. 8, showing the universal curve for $c_{\text{eff}}(\tau)$. The high accuracy of this collapse can be checked in the inset, which shows the same data in logarithmic scale. Moreover, the circles correspond to the plot of c_{eff} in Eq. (24) as a function of $\ln(\tau)$, for comparison.

D. Phase diagram

In Fig. 9, we show the relative error between the theoretical prediction and the numerics

$$\delta s(h,\gamma) = \frac{|s(h,\gamma) - hc_{\text{eff}}|}{s(h,\gamma)}, \tag{38}$$

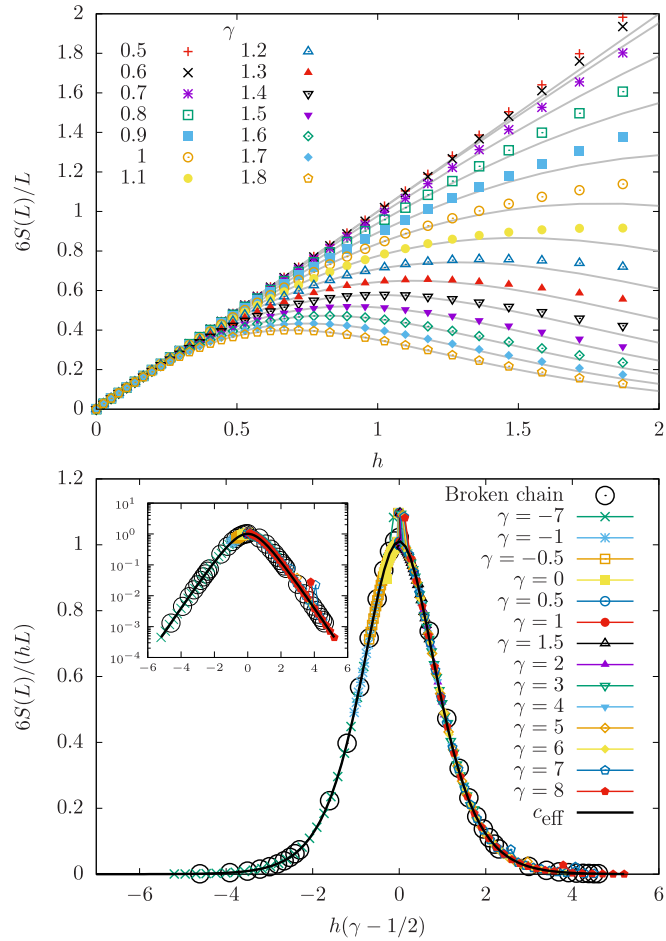

FIG. 8. (Top) Entropy per site of the rainbow model with a defect, $s(h,\gamma)$ as a function of h, for different values of γ. Soft continuous lines correspond to the theoretical prediction, Eq. (36). (Bottom) Entropy per site divided by the inhomogeneity parameter, as a function of the defect intensity, $h(\gamma - 1/2)$, showing the collapse predicted by Eq. (36).

in the color intensity. The white lines correspond to the theoretical values of the relative maxima of $s(h,\gamma)$ as a function of h, following Eq. (36). Notice that the theoretical prediction states that, for all γ, the curve $s(h)$ will present a maximum and decay to zero afterwards. Thus weak inhomogeneity regime presents a smooth crossover into the three phases of the strong inhomogeneity regime described in the previous section or large h lattice effects become dominant and the universal properties predicted by the field theory approach are lost.

E. Beyond entanglement entropy

The characterization of entanglement can be improved with the study of the entanglement spectrum (ES), entanglement contour and entanglement Hamiltonian. All these mathematical objects are associated to the reduced density matrix of the block, ρ_A.

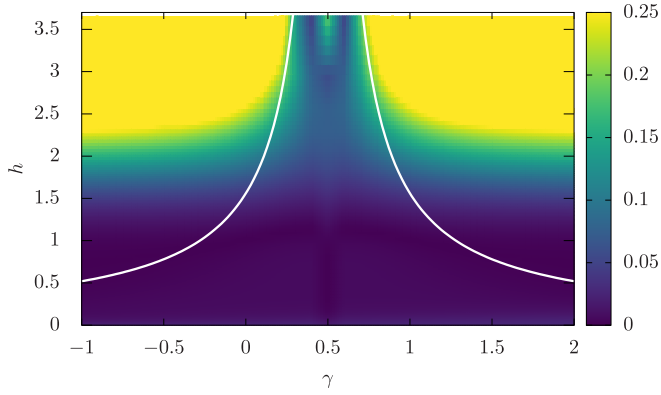

FIG. 9. Phase diagram, absolute error of the EE prediction; the white lines correspond to the local maximum of the entropy density, $s(h)$.

1. Entanglement Hamiltonian

The reduced density matrix ρ_A of a Gaussian fermionic state can be written in the form

$$\rho_A = \exp(-2\pi H_A) \equiv \exp\left(-2\pi \sum_p \epsilon_p d_p^\dagger d_p\right), \tag{39}$$

for some fermionic operators d_p. The ϵ_p are called the single-body entanglement spectrum, but the term single body is usually dropped. Operator H_A is termed the entanglement Hamiltonian (EH), and it can be shown to be approximately local for a 1+1D CFT [28]. Indeed, it can be written as

$$H_A \approx \sum_i \beta_A(i)\, c_i^\dagger c_{i+1}, \tag{40}$$

where the $\beta_A(i)$ constitute entanglement couplings, and can be accounted for in CFT providing an extension of the Bisognano-Wichmann theorem [28,42]. There are also nonzero terms presenting long-range interactions, but they are expected to be very small. The estimation of the set of β_i is obtained by minimizing an error function $E(\beta) \equiv \sum_{i,j\in A} (C_{ij} - Tr(\rho_A(\beta) c_i^\dagger c_j))$ using standard optimization techniques [28].

The numerical values of $\{\beta(i)\}$ for the left half (block A_L) of a $L = 20$ system, using $h = 0.5$ and different values of γ are shown in Fig. 10. For $\gamma = 1/2$ the EH of the rainbow system presents flat coefficients $\beta(i)$ everywhere except near the physical boundary (left extreme) and near the internal boundary (right extreme), where it follows the Bisognano-Wichmann prediction, that they will decay to zero linearly, with slope 1. Yet, in presence of a defect we observe an increasing dimerization of the EH.

Let us remind the reader that the flat profile for $\{\beta(i)\}$ in the rainbow case accounts for the fact that the rainbow GS for all values of h resembles a thermofield double [28], i.e.,

$$|\Psi\rangle \approx \sum_n \exp(-\beta E_n/2)|n\rangle_L \otimes |n\rangle_R, \tag{41}$$

where E_n and $|n\rangle_{\{L,R\}}$ are the energies and eigenstates of the homogeneous free Hamiltonian on the left/right with open boundaries. Thus we are led to the following claim: in presence of a defect, the ground state of Hamiltonian (2) is

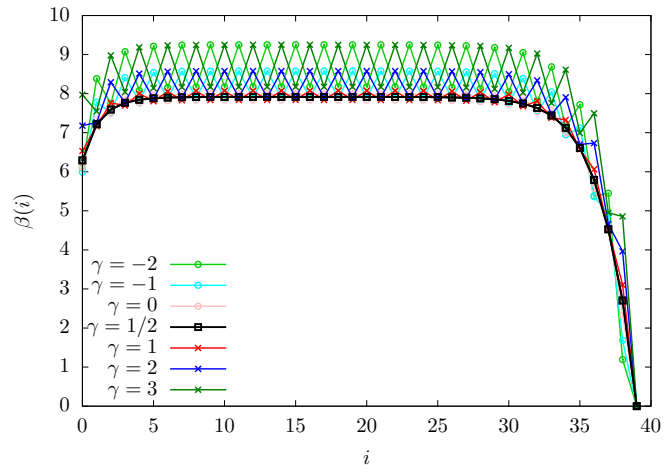

FIG. 10. Entanglement Hamiltonian coefficients $\{\beta(i)\}$ for the left half of a $L = 20$ rainbow with a defect, using $h = 0.5$. Notice that, for $\gamma = 1/2$, the bulk is flat, as expected, but for the other values the Hamiltonian coefficients present dimerization, which changes the high and low values when we change γ for $1 - \gamma$.

still approximately a thermofield double, but of a dimerized Hamiltonian, with dimerization parameter associated to the defect strength γ. We would like to stress that the cases of γ and $1 - \gamma$ are extremely similar, only interchanging the higher and lower values of the dimerization pattern.

2. Entanglement spectrum

For free systems, the entanglement spectrum (ES) $\{\epsilon_k\}_{k=1}^L$ of a block A is the single-body spectrum of the reduced density matrix ρ_A [43]. In terms of the ES, the eigenvalues $\{\nu_k\}_{k=1}^L$ of the block correlator matrix are written [38] as

$$\nu_k = \frac{1}{e^{\epsilon_k} + 1}. \tag{42}$$

The ES contains more physical information than the entanglement entropy. In some cases, its low part can be regarded as the energy spectrum of a boundary CFT [44].

We have considered the full ES of the left half block, A_L, for different values of γ. As it can be expected, the defect preserves the particle-hole symmetry. The most salient feature is that the ES shows a finite gap $\Delta\epsilon$ whose width grows with γ, as can be seen in Fig. 11 (top). For a CFT system, the entanglement gap, $\Delta\epsilon \sim 1/\ln(L)$, but for a deformed system such as the rainbow we should consider instead $\Delta\epsilon \sim 1/\ln(\tilde{L}) \sim 1/L$. Indeed, for low h the gap decays linearly with the system size, as we can see on the bottom panel of Fig. 11 for $h = 0.015$, but it seems to reach a finite value for $h = 0.32$.

3. Entanglement contour

The entanglement contour [45] attempts to answer the question about where is the entanglement entropy located. The entanglement entropy of a block is decomposed

$$S_A = \sum_{i\in A} \sigma_A(i), \tag{43}$$

with $\sigma_A(i) \geqslant 0$. Although the entanglement contour is not uniquely defined, different candidate definitions have

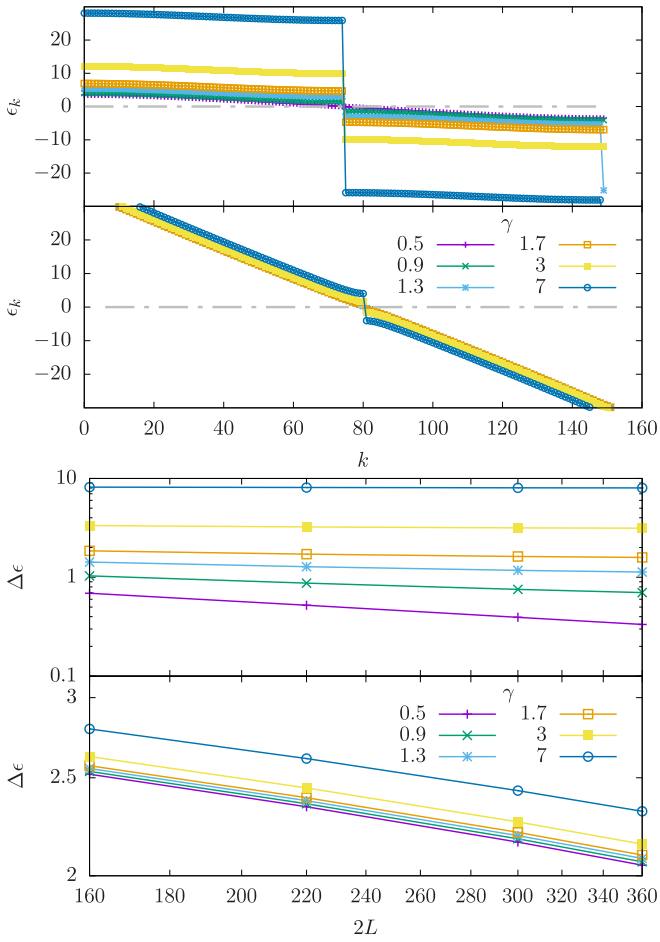

FIG. 11. (Top) Entanglement spectrum ϵ_k of the left block of a system with $L = 150$ and different values of γ: (top) $h = 0.32$ and (bottom) 0.015. (Bottom) Scaling of the ES gap $\Delta\epsilon$ with size $2L$ for different values of γ: (top) $h = 0.32$ and (bottom) 0.015.

provided very similar values [28,46,47], thus pointing at the existence of a deeper contour which would have the current candidates as approximations. Since the rainbow system is defined here for a free-fermionic system, we will employ the approach given in [45].

Figure 12 shows the curve of the entanglement contour for the left block of the rainbow GS using $L = 40$ and $h = 0.5$, for different values of γ, scaled with the entropy density predicted in Eq. (36). The collapse is very clear in the bulk region, which presents universal features, and a little bit less near the boundary, where it does not. Importantly, notice that the entanglement contour does not present any oscillations related to dimerization, with a constant entropy per site in the bulk.

V. DEFECT IN A SYMMETRY PROTECTED TOPOLOGICAL PHASE

The system considered so far, Eq. (2), presents bond centered symmetry, i.e., the center of symmetry is in the middle point of the central link. However, many different properties arise when we consider site centered symmetric (scs) systems [22], where the center of symmetry corresponds to a site. Let us consider a system defined on a chain with

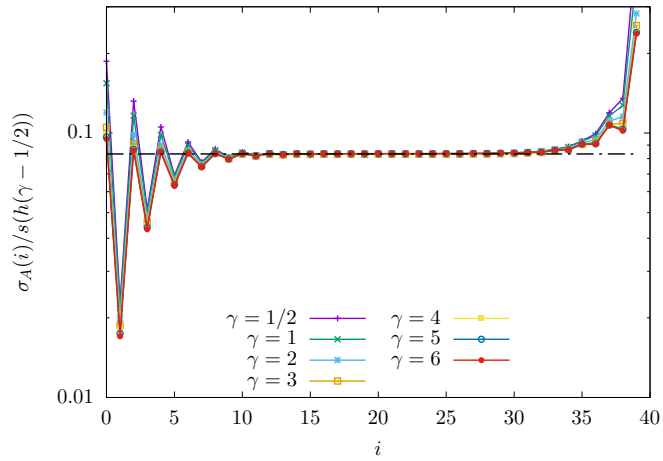

FIG. 12. Entanglement contour of the left half (the left edge is the physical boundary while the right one is originated by the block) of the rainbow model with a defect using $L = 40$ and $h = 0.5$, scaled with the entropy per site predicted in Eq. (36), for different values of γ.

$N = 2L$ sites, whose Hamiltonian is

$$H_N(h,\gamma)_{\text{scs}} = -\frac{1}{2}\sum_{m=1}^{N} J_m c_m^\dagger c_{m+1} + \text{H.c.}, \tag{44}$$

where the fermions are now placed on integer positions and there are two equal central hoppings depending on γ:

$$J_m = \begin{cases} e^{-h(|m-(L+\frac{1}{2})|-\frac{1}{2})} & \text{if } m \neq L, L+1, \\ e^{-h\gamma} & \text{if } m \in \{L, L+1\}, \end{cases} \tag{45}$$

i.e., the log-couplings (see Eq. (A1)) present the pattern $\{\ldots, 3, 2, 1, \gamma, \gamma, 1, 2, 3, \ldots\}$. The site-centered symmetry manifests itself through the invariance of the hoppings under an inversion around the central site $L+1$: $J_n = J_{L+1-n}$. Notice that the new notation is different from the bond centered symmetry case, Eq. (2), which is now convenient due to the different type of symmetry.

In Ref. [22], it was shown that after performing a folding operation around the central site, the system becomes an inhomogeneous realization of the SSH model, thus belonging to the BDI class of topological phases [48–55]. Since the topological nature of the state is highlighted after removing the local entanglement [54], it is better to study the system in the strong inhomogeneity regime. The fermionic excitations are not spread along the whole system as it is the case in the weak inhomogeneity limit. Hence, we will study the system in the strong coupling regime $H_N(h \gg 1, \gamma)_{\text{scs}}$ by means of renormalization schemes that depend on the value of γ (see details in Appendix F).

Let us start by considering the case $\gamma \leqslant 1$. The dominant interaction involves the three central sites, L, $L+1$, and $L+2$. With a real-space first-order perturbation theory RG [22]. On each step, three fermions are truncated into one which participates on the next step (unlike the RG of the systems with bcs symmetry, where the fermions are integrated out on each step and hence are decoupled from the system) leading to a topological ground state with non removable entanglement

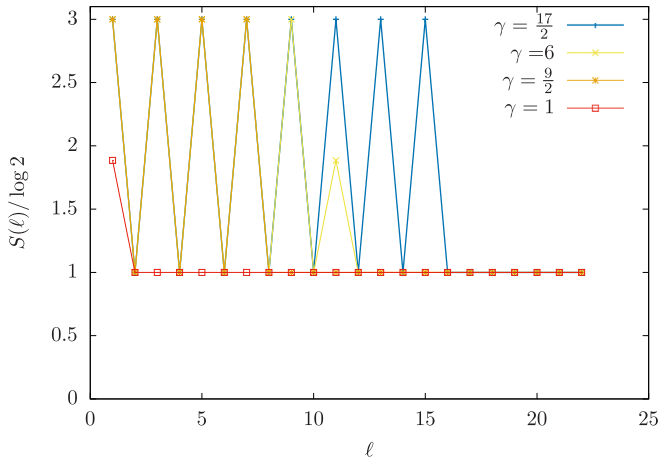

FIG. 13. Entanglement entropy of the system with Hamiltonian $H_{46}(15, \gamma)_{\text{scs}}$ partitioned with central blocks B_ℓ for different values of γ. The entropy is $S[B_\ell] = 3 \ln 2$ if $\ell < \lfloor \gamma \rfloor$ and it is $S[B_\ell] = \ln 2$ if $\ell > \lfloor \gamma \rfloor$. If $\gamma \in \mathbb{N}$, $S[B_{\ell=\gamma}]$ takes another value which is a consequence of the quadruple tie that we have discussed in the text.

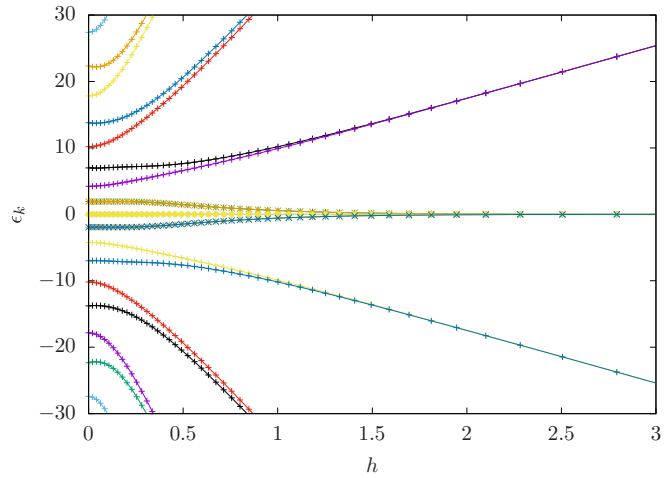

FIG. 14. Single body entanglement spectrum ϵ_k of a block B_{11} of a system described by the Hamiltonian $H_{46}(h, \frac{17}{2})_{\text{scs}}$ as a function of h. Notice the topological zero mode, which does not depend on h.

that belongs to the BDI class [22,49]. The case with $\gamma = 1$ differs only on the first step of the RG where five spins (instead of three) are truncated to one.

On the other hand, the case $\gamma > 1$ is again different. Starting from $H_N(h, \gamma)_{\text{scs}}$, the dominant interactions are two non consecutive log-couplings 1 which allows the use of the Dasgupta-Ma RG (A2), leading to an effective system whose Hamiltonian is $H_{N-4}(h, 1+\gamma)_{\text{scs}}$. If $1+\gamma$ happens to be the dominant interaction, three fermions are involved so the Dasgupta-Ma Rg is not applicable anymore and the way of procedure is described in the previous paragraph. On the contrary, if the log-couplings 2 are the dominant interaction, the Dasgupta-Ma RG can be applied again leading to a new Hamiltonian $H_{N-8}(h, 2+\gamma)_{\text{scs}}$. Hence, the same dichotomy is present in the next step. The procedure iterates and unless $\gamma > L-1$ the RG flows eventually to a dominant interaction which involves three fermions.

Therefore we see that the GS of the Hamiltonian $H_N(h, \gamma > 1)_{\text{scs}}$ is obtained via the application of two kinds of renormalization group schemes. As a consequence, the ground state of this Hamiltonian has two different phases that coexist: a dimerized phase around the defect and the BDI phase away from it. This coexistence is well captured by considering the EE of central blocks $B_\ell = \{L-\ell, L+2+\ell\}$, with $\ell \in \{0, \ldots, (L-1)\}$. Since the system is topologically nontrivial, there is entanglement that cannot be removed (the EE in bounded by $\ln 2$ for all B_ℓ) and for blocks B_ℓ with $\ell \in \{0, \ldots, (L-1)\}$ as can be seen in Fig. 13. $\ell < \lfloor \gamma \rfloor$, $SB_\ell = 3 \ln 2$ due to the fact that there are two fermionic excitations $b^\dagger_{L-2(\ell-1),L-2(\ell-1)-1}|0\rangle$ and $b^\dagger_{L+2\ell,L+2\ell+1}|0\rangle$ that are not fully contained in the block B_ℓ. Furthermore, the dimerized phase appears only in the strong inhomogeneity limit $h \to \infty$ while the BDI phase is independent of the inhomogeneity parameter. This fact can be checked by considering the behavior of the single body entanglement spectrum ϵ_k, see Fig. 14 and Eq. (42). There is a zero mode $\epsilon_0 = 0$ for all h that gives rise to a double degeneracy of the many-body entanglement spectrum and it is a signature of the topological nature of the state. There are also two additional zero modes due to the presence of the defect but they are not topological, since they depend on the inhomogeneity.

VI. CONCLUSIONS AND FURTHER WORK

In this work, we have characterized a lattice model of Dirac fermions on a negatively curved background in presence of a local defect. The unperturbed lattice model is the so-called rainbow model, which is a free-fermionic chain with hoppings which decay exponentially from the center. Its ground state presents linear growth of the entanglement, with an entropy per site proportional to the inhomogeneity parameter h in the weak inhomogeneity regime, which is described by a geometrical deformation of the free-fermionic conformal field theory, associated to a hyperbolic space-time metric. The strong inhomogeneity limit is described as a valence bond state with concentric bonds around the center, as it can be established using the Dasgupta-Ma renormalization group.

The presence of a defect in the center of the chain can induce an entanglement transition in the strong inhomogeneity limit, characterized by a rainbow phase of linear scaling of entanglement for intermediate defect strengths, and two dimerized phases, with alternate dimerizations in similarity with the SSH model. Further hints of the transition are provided by the ground state energy, the single-body orbitals, the energy gap (rescaled with the minimum coupling) and two-order parameters: the average dimerization and the rainbow order parameter, which measures the average occupation of the concentric bonds.

In the weak inhomogeneity limit, the transition gets blurred, and the ground state always presents linear entanglement, with an entropy per site that can be effectively described by a geometric deformation of the entanglement entropy of a homogeneous fermionic chain with a central defect. Analysis of the entanglement gap and the entanglement Hamiltonian allow us to claim that the system behaves as a thermofield double, as in the rainbow case, but with a dimerized Hamiltonian instead of a homogeneous one.

Interestingly, the rainbow system presents nontrivial topological properties when it is centered on a site instead of a link. In presence of a defect, the ground state presents an interesting coexistence of a symmetry-protected topological phase near the ends and a dimerized region near the center, whose size grows as the defect intensity goes to zero.

Our work opens up several interesting questions related to the presence of geometric defects on the vacuum structure of a quantum field theory. It is interesting to ask whether such a deep modification of the entanglement properties can be found in other cases.

ACKNOWLEDGMENTS

We thank A. Dauphin, J. I. Latorre, A. Ludwig, S. Ryu, and E. Tonni for conversations. We acknowledge the Spanish government for financial support through Grants No. PGC2018-095862-B-C21 (NSSB and GS), No. FIS2015-66020-C2-1-P and No. PGC2018-094763-B-I00 (SNS), QUITEMAD+ S2013/ICE-2801, SEV-2016-0597 of the "Centro de Excelencia Severo Ochoa" Programme and the CSIC Research Platform on Quantum Technologies PTI-001.

APPENDIX A: DETAILS OF THE APPLICATION OF THE SDRG

In this Appendix, we detail the obtention of the ground states by using the SDRG. For our purposes, it is convenient to define the log-couplings [23] of the original couplings J_i (3):

$$t_i = -\ln \frac{|J_i|}{h}, \tag{A1}$$

where h is the inhomogeneity parameter that is included for later convenience. In this language, the two fermionic sites that are integrated out on each step of the RG are those connected by the lowest t_i and the effective coupling Eq. (5) is computed in additive way:

$$\tilde{t}_i = t_{i-1} - t_i + t_{i+1}. \tag{A2}$$

Interestingly, Eq. (A2) can be generalized for this type of models: whenever a bond is established between sites p and q (with $p+q$ even), the renormalized log-coupling is given by the sum rule [24]:

$$\tilde{t}_{[p,q]} = \sum_{j=0}^{q-p-1} (-1)^j t_{p+j}, \tag{A3}$$

or, in other words: the renormalized log-coupling can be obtained summing all log-coupling between the two extremes, with alternating signs.

(1) The rainbow phase: $\gamma \in (0,1)$, see Fig. 2(b). The strongest link (lowest log-coupling) is the central one. Thus a valence bond is established on top ($b^+_{-1/2,+1/2}$) and an effective log-coupling appears between its neighbors, of magnitude $\tilde{t} = 2-\gamma < 2$. Thus the central link is again the strongest one, so we can put a valence bond on top of it ($b^-_{-3/2,+3/2}$), leading to an effective log-coupling of magnitude $\tilde{t} = 2+\gamma < 3$. We can see that the procedure iterates, giving rise to the rainbow state.

$$|\mathrm{GS}\rangle_{\gamma\in(0,1)} = \prod_{i=0}^{L-1} \left(b^{\eta_i}_{-i-1/2,i+1/2}\right)^\dagger |0\rangle, \quad \eta_i = (-1)^i. \tag{A4}$$

(2) The dimerized phase (I): $\gamma < 0$, see Fig. 2(c). The dominant interaction is again the central one, leading us to establish a valence bond on top. Yet, the renormalized log-coupling, $\tilde{t} = 2-\gamma > 2$ is not the strongest (lowest value) at the next SDRG iteration. On the other hand, we are led to establish two valence bonds on top of the links with log-couplings equal to 2, in any order. The renormalized central log-coupling after these two bonds have been established is $\tilde{t} = 4-\gamma > 4$ [see Eq. (A3)], so we are led to the same situation, where the lateral links are always stronger than the central one, leading to a dimerized state. Yet, the last SDRG step leaves us with the two extreme sites of the chain, leading to a final bond connecting them. The ground state can be written as

$$|\mathrm{GS}\rangle_{\gamma<0} = (b^-_{-L+\frac{1}{2},L-\frac{1}{2}})^\dagger \prod_{i=-\frac{L}{2}+1}^{\frac{L}{2}-1} (b^+_{2i-\frac{1}{2},2i+\frac{1}{2}})^\dagger |0\rangle. \tag{A5}$$

Notice that the last bond is only present for even L, while it is absent for odd L.

(3) The dimerized phase (II): $\gamma > 1$, see Fig. 2(d). In this case, the dominant interaction is not the central one, but their neighbors, with $t_{\pm1} = 1$. Hence, we must establish first these two valence bonds, leading to a renormalized log-coupling between their extremes of $\tilde{t} = 2+\gamma > 3$ [see Eq. (A3)]. Thus we have the same situation, in which the central link is not the strongest. In this case, no long-range bond is established at the end of the procedure, and we obtain

$$|\mathrm{GS}\rangle_{\gamma>1} = \prod_{i=-\frac{L-1}{2}}^{\frac{L-1}{2}} (b^+_{2i-\frac{1}{2},2i+\frac{1}{2}})^\dagger |0\rangle. \tag{A6}$$

(4) The transition points: $\gamma = 1$ and $\gamma = 0$, see Figs. 2(e) and 2(f). Let us start with $\gamma = 1$ [Fig. 2(e)]. The first SDRG step fails, because the strongest coupling is not unique. On the other hand, we obtain a triple tie in the three central links, with $t_{0,\pm1} = 1$. In Appendix B, we have developed an extension of the SDRG for the free-fermion model when a block with 2ℓ sites is integrated out, yielding the renormalized log-coupling given by the sum rule, Eq. (A3). Thus the renormalized log-coupling between sites $-5/2$ and $+5/2$ is $\tilde{t} = 3$, leading to a new triple tie, which propagates further along the chain. For $\gamma = 0$, on the other hand, the strongest link is the central one, thus receiving a valence bond. But, on the next SDRG step, we can see that the effective central log-coupling is $\tilde{t} = 2$, equal to its neighbors in a new triple tie, forcing us to recourse to the extended SDRG. From that moment on, all SDRG steps lead to triple ties. The GS can be written exactly in these two cases

(see details in Appendix C)

$$|\mathrm{GS}\rangle_{\gamma=0} = (b^{-}_{-L+\frac{1}{2},L-\frac{1}{2}})^{\dagger}\prod_{i=1}^{\frac{L}{4}}(d^{\eta_i}_{2i+\frac{1}{2}})^{\dagger}(b^{+}_{-\frac{1}{2},\frac{1}{2}})^{\dagger}|0\rangle, \quad \text{(A7)}$$

$$|\mathrm{GS}\rangle_{\gamma=1} = \prod_{i=1}^{\frac{L}{2}}(d^{\eta_i}_{2i-\frac{1}{2}})^{\dagger}|0\rangle, \quad \text{(A8)}$$

where $d^{\pm}_{k}$ is operators creating two particles on four fermionic sites,

$$(d^{\eta_i}_{i})^{\dagger} = (v^{\eta_i})^{\dagger}(u^{\eta_{i-1}})^{\dagger}|0\rangle, \quad \eta_i = (-1)^i, \quad \text{(A9)}$$

$$u^{\pm}_{i} = \frac{1}{\sqrt{5+\sqrt{5}}}(c_{-i} \pm c_i) + \frac{1}{\sqrt{5-\sqrt{5}}}(c_{-i+1} \pm c_{i-1}), \quad \text{(A10)}$$

$$v^{\pm}_{i} = \frac{1}{\sqrt{5-\sqrt{5}}}(c_{-i} \pm c_i) + \frac{1}{\sqrt{5+\sqrt{5}}}(c_{-i+1} \pm c_{i-1}). \quad \text{(A11)}$$

APPENDIX B: DASGUPTA-MA RG EXTENSION FOR FREE FERMIONS

In this Appendix, we describe a generalization of the Dasgupta-Ma RG for inhomogeneous free fermionic chains that can be applied to systems that have an homogeneous subchain of $N = 2L$ sites embedded. The Hamiltonian H_0 that describes this subchain is given by

$$H_0 = -\frac{J}{2}\sum_{i=1}^{N-1} c^{\dagger}_{i}c_{i+1} + c^{\dagger}_{i+1}c_i, \quad \text{(B1)}$$

and its interactions with the nearest neighbours is given by H_{lr}

$$H_{lr} = -J_l c^{\dagger}_{l}c_1 - J_r c^{\dagger}_{N}c_r + \mathrm{H.c.} \quad \text{(B2)}$$

Assuming that $J_l \ll J$ and $\frac{J_l}{J_r} \approx 1$, the whole system can be study by means of degenerate perturbation theory. The ground state of H_0 is given in the previous Appendix C $|\psi_0\rangle = \prod_{m=1}^{L}\hat{\phi}^{\dagger}_{k_m}|0\rangle$ with energy $E_0 = \sum_{m=1}^{L}\epsilon_{k_m} = -2\sum_{m=1}^{L}\cos\left(\frac{m\pi}{N+1}\right)$. The first-order correction $\langle\psi_0; l', r'|H_{lr}|\psi_0; l, r\rangle$ (where $|\psi_i; l, r\rangle = |\psi_i\rangle \otimes |l\rangle \otimes |r\rangle$) vanishes. The matrix element $B_{l,r;l'r'}$ of the degenerate second order contribution is given by

$$B_{l,r;l'r'} = \sum_{i\neq 0}\sum_{l''r''}\frac{\langle\psi_0; l, r|H_{lr}|\psi_i; l'', r''\rangle\langle\psi_i; l'', r''|H_{lr}|\psi_0; l', r'\rangle}{E_0 - E_i}. \quad \text{(B3)}$$

Expanding this product and taking into account that $\sum_{l''r''}|l'', r''\rangle\langle l'', r''| = \mathbb{I}$, we have

$$\begin{aligned}
B_{l,r;l'r'} = {} & J_l^2\left(\langle l, r|c^{\dagger}_{l}c_l|l', r'\rangle\sum_{i=1}^{N}\frac{\langle\psi_0|c_1|\psi_i\rangle\langle\psi_i|c^{\dagger}_{1}|\psi_0\rangle + \langle\psi_0|c^{\dagger}_{1}|\psi_i\rangle\langle\psi_i|c_1|\psi_0\rangle}{\epsilon_{k_i}} - \sum_{i=1}^{N}\frac{\langle\psi_0|c^{\dagger}_{1}|\psi_i\rangle\langle\psi_i|c_1|\psi_0\rangle}{\epsilon_{k_i}}\right) \\
& + J_r^2\left(\langle l, r|c^{\dagger}_{r}c_r|l', r'\rangle\sum_{i=1}^{N}\frac{\langle\psi_0|c_N|\psi_i\rangle\langle\psi_i|c^{\dagger}_{N}|\psi_0\rangle + \langle\psi_0|c^{\dagger}_{N}|\psi_i\rangle\langle\psi_i|c_N|\psi_0\rangle}{\epsilon_{k_i}} - \sum_{i=1}^{N}\frac{\langle\psi_0|c^{\dagger}_{N}|\psi_i\rangle\langle\psi_i|c_N|\psi_0\rangle}{\epsilon_{k_i}}\right) \\
& + J_l J_r\left(\langle l, r|c^{\dagger}_{l}c_r|l', r'\rangle\sum_{i=1}^{N}\frac{\langle\psi_0|c_1|\psi_i\rangle\langle\psi_i|c^{\dagger}_{N}|\psi_0\rangle + \langle\psi_0|c^{\dagger}_{N}|\psi_i\rangle\langle\psi_i|c_1|\psi_0\rangle}{\epsilon_{k_i}}\right. \\
& \left. + \langle l, r|c^{\dagger}_{r}c_l|l', r'\rangle\sum_{i=1}^{N}\frac{\langle\psi_0|c_N|\psi_i\rangle\langle\psi_i|c^{\dagger}_{1}|\psi_0\rangle + \langle\psi_0|c^{\dagger}_{1}|\psi_i\rangle\langle\psi_i|c_N|\psi_0\rangle}{\epsilon_{k_i}}\right),
\end{aligned} \quad \text{(B4)}$$

where the nonvanishing contributions are given by the excited states whose particle number differs by one with respect to $|\psi_0\rangle$:

$$\langle\psi_i|c^{\dagger}_{i}|\psi_0\rangle \neq 0 \quad \text{if} \quad |\psi_i\rangle = \hat{\phi}_{k_i}|\psi_0\rangle, \quad E_i = E_0 - \epsilon_{k_i}, \quad \text{(B5)}$$

$$\langle\psi_i|c_i|\psi_0\rangle \neq 0 \quad \text{if} \quad |\psi_i\rangle = \hat{\phi}^{\dagger}_{k_i}|\psi_0\rangle, \quad E_i = E_0 + \epsilon_{k_i}\,. \quad \text{(B6)}$$

Given that $c_i = \sum_{m=1}^{N} f^{*}_{im}\hat{\phi}_{k_m}$, we reach

$$\begin{aligned}
B_{l,r;l'r'} = {} & J_l^2\left(\langle l, r|c^{\dagger}_{l}c_l|l', r'\rangle\sum_{i=1}^{N}\frac{|f_{1m}|^2}{\epsilon_{k_m}} + \sum_{i=1}^{L}\frac{|f_{1m}|^2}{\epsilon_{k_m}}\right) + J_r^2\left(\langle l, r|c^{\dagger}_{r}c_r|l', r'\rangle\sum_{i=1}^{N}\frac{|f_{Nm}|^2}{\epsilon_{k_m}} + \sum_{i=1}^{L}\frac{|f_{Nm}|^2}{\epsilon_{k_m}}\right) \\
& + J_l J_r\left(\langle l, r|c^{\dagger}_{l}c_r|l', r'\rangle\sum_{i=1}^{N}\frac{f^{*}_{1m}f_{mN}}{\epsilon_{k_m}} + \langle l, r|c^{\dagger}_{r}c_l|l', r'\rangle\sum_{i=1}^{N}\frac{f^{*}_{Nm}f_{m1}}{\epsilon_{k_m}}\right).
\end{aligned}$$

Now, particularizing for the functions Eq. (C1) we obtain that the renormalized Hamiltonian B is (up to an additive constant):

$$H_{\mathrm{eff}} = -\frac{J_l J_r}{J}(c^{\dagger}_{l}c_r + \mathrm{H.c}), \quad \text{(B7)}$$

which is the expression used to renormalize the systems with strength defects $\gamma = 0$ and $\gamma = 1$.

APPENDIX C: THE TRANSITION BLOCKS: $\gamma = 1$ AND $\gamma = 0$.

In this Appendix, we derive Eq. (8). Consider an homogeneous system of $N = 2L$ sites with open boundary conditions whose Hamiltonian is given by Eq. (B1). Solving the time independent Schrödinger equation $H_0|\phi_k\rangle = \epsilon_k|\phi_k\rangle$, we arrive at

$$\epsilon_{k_m} = -J\cos\left(\frac{m\pi}{N+1}\right),$$

$$|\phi_{k_m}\rangle = \hat{\phi}^\dagger_{k_m}|0\rangle = \sum_{i=1}^{N} f^*_{mi}c^\dagger_i|0\rangle,$$

$$\text{within } f^*_{mi} = \sqrt{\frac{2}{N+1}}\sin\left(\frac{m\pi i}{N+1}\right). \tag{C1}$$

Taking $N = 4$, the many body ground state $|\psi\rangle$ at half filling is obtained by occupying the single body levels with energies $-J\cos\frac{\pi}{5}$ and $-J\cos\frac{2\pi}{5}$.

$$|\psi_0\rangle = d^\dagger|0\rangle = v^\dagger u^\dagger|0\rangle = \hat{\phi}^\dagger_{k_2}\hat{\phi}^\dagger_{k_1}|0\rangle. \tag{C2}$$

APPENDIX D: CORRELATION MATRICES AND ENTANGLEMENT ENTROPY

The correlation matrices C for the ground states Eqs. (A4)–(A8) are given by

$$C_{ij} = \langle \mathrm{GS}|\mathrm{c}^\dagger_\mathrm{i}\mathrm{c}_\mathrm{j}|\mathrm{GS}\rangle = \sum_{\mathrm{m,m'=1}}^{\mathrm{L}} \mathrm{f_{i,m}f^*_{m',j}}\langle \mathrm{GS}|\hat{\phi}^\dagger_\mathrm{m}\hat{\phi}_\mathrm{m'}|\mathrm{GS}\rangle$$

$$= \sum_{m=1}^{L} f_{i,m}f^*_{m,j}, \tag{D1}$$

where we consider half filling and $\hat{\phi}_m$ are the fermionic excitations of each system [$b_{i,j}$ Eq. (7) and d_i Eq. (8) in our case] and $f_{i,k}$ is a unitary matrix.

The EE entropy of a block A_ℓ is given by [38]

$$S(A_\ell) = -\sum_{k=1}^{\ell} \nu_k \ln \nu_k + (1-\nu_k)\ln(1-\nu_k), \tag{D2}$$

where the $\{\nu_k\}$ are the set of eigenvalues of the correlation matrix restricted to the block A_ℓ. We shall next describe the correlation matrices as a function of the defect parameter γ. All the matrices are symmetric $C_{i,j} = C_{j,i}$ and present left-right symmetry $C_{i,j} = C_{N+1-j,N+1-i}$. All the computations are done with L even.

(1) $\gamma < 0$:

$$\begin{cases} C_{i,i} = \frac{1}{2}, & i = 1,\dots,L, \\ C_{1,N} = -\frac{1}{2}, & \\ C_{2i,2i+1} = \frac{1}{2}, & i = 1,\dots\frac{L}{2}. \end{cases} \tag{D3}$$

(2) $\gamma = 0$:

$$\begin{cases} C_{1,N} = -\frac{1}{2}, & C_{L,L+1} = \frac{1}{2} \\ C_{i,i} = \frac{1}{2}, & i = 1,\dots,L \\ C_{i,N+1-i} = (-1)^i\frac{1}{2\sqrt{5}}, & i = 2,\dots,L-1 \\ C_{2i,2i+1} = \frac{1}{\sqrt{5}}, & i = 1,\dots\frac{L}{2}. \end{cases} \tag{D4}$$

(3) $\gamma \in (0,1)$:

$$C_{i,j} = \tfrac{1}{2}\delta_{i,i} + (-1)^i\tfrac{1}{2}\delta_{i,N+1-i}. \tag{D5}$$

(4) $\gamma = 1$:

$$\begin{cases} C_{i,i} = \frac{1}{2}, & i = 1,\dots,L, \\ C_{i,N+1-i} = (-1)^i\frac{1}{2\sqrt{5}}, & i = 1,\dots,L, \\ C_{2i-1,2i} = \frac{1}{\sqrt{5}}, & i = 1,\dots\frac{L}{2}. \end{cases} \tag{D6}$$

(5) $\gamma > 1$:

$$\begin{cases} C_{i,i} = \frac{1}{2}, & i = 1,\dots,L, \\ C_{2i-1,2i} = \frac{1}{2}, & i = 1,\dots\frac{L}{2}. \end{cases} \tag{D7}$$

The correlation matrix of the four sites that are integrated out in the same step whose ground state is given by Eq. (8) is

$$C_4 = \begin{pmatrix} \frac{1}{2} & \frac{1}{\sqrt{5}} & 0 & -\frac{1}{2\sqrt{5}} \\ \frac{1}{\sqrt{5}} & \frac{1}{2} & \frac{1}{2\sqrt{5}} & 0 \\ 0 & \frac{1}{2\sqrt{5}} & \frac{1}{2} & \frac{1}{\sqrt{5}} \\ -\frac{1}{2\sqrt{5}} & 0 & \frac{1}{\sqrt{5}} & \frac{1}{2} \end{pmatrix}. \tag{D8}$$

The most simple non trivial lateral block is

$$A_2 = \begin{pmatrix} \frac{1}{2} & \frac{1}{\sqrt{5}} \\ \frac{1}{\sqrt{5}} & \frac{1}{2} \end{pmatrix}, \tag{D9}$$

whose eigenvalues are $\nu_1 = \frac{1}{10}(2\sqrt{5}+5)$, $\nu_2 = \frac{1}{10}(5-2\sqrt{5})$. The value of S_a, given in Eq. (15), is obtained applying Eq. (D2). Furthermore S_b, given in Eq. (16), is obtained from the central block

$$B_1 = \begin{pmatrix} \frac{1}{2} & \frac{1}{2\sqrt{5}} \\ \frac{1}{2\sqrt{5}} & \frac{1}{2} \end{pmatrix}, \tag{D10}$$

whose eigenvalues are $\nu_1 = \frac{1}{10}(\sqrt{5}+5)$, $\nu_2 = \frac{1}{10}(5-\sqrt{5})$. It can be shown that larger central blocks have also these nontrivial eigenvalues and the rest are 0 and 1 which don't contribute to the EE.

APPENDIX E: RELATION WITH DIRAC EQUATION WITH δ POTENTIAL

Consider an inhomogeneous free-fermion chain with a central hopping defect and bond centered symmetry described by the Hamiltonian:

$$H(\tau) = -\frac{\tau}{2}c^\dagger_{-\frac{1}{2}}c_{\frac{1}{2}} - \frac{1}{2}\sum_{m=\frac{1}{2}}^{L-\frac{3}{2}} J_m(c^\dagger_m c_{m+1} + c^\dagger_{-m}c_{-m+1}). \tag{E1}$$

The single body spectrum is obtained by diagonalizing the hopping matrix. The eigenvalue equations at the center of the chain are

$$\alpha\phi_{-\frac{3}{2}} + \tau\phi_{\frac{1}{2}} = \epsilon\phi_{-\frac{1}{2}}, \tag{E2}$$

$$\tau\phi_{-\frac{1}{2}} + \alpha\phi_{\frac{3}{2}} = \epsilon\phi_{\frac{1}{2}}, \tag{E3}$$

where ϵ is the single body energy and ϕ_m is the amplitude associated with the fermionic operator c_m and $J_{\frac{1}{2}} = \alpha$. The

expansion of the local operators c_m in terms of its right and left moving components around the Fermi points [see Eq. (18)] leads to the equations

$$\tau\left(\psi_L^{II} - i\psi_R^{II}\right) = (-i\epsilon + \alpha)\psi_L^I + (\epsilon - i\alpha)\psi_R^I, \tag{E4}$$

$$\tau\left(\psi_L^{I} + i\psi_R^{I}\right) = (i\epsilon + \alpha)\psi_L^{II} + (\epsilon + i\alpha)\psi_R^{II}, \tag{E5}$$

with

$$\lim_{a\to 0}\psi_{L,R}\left(-\tfrac{3}{2}a\right) = \lim_{a\to 0}\psi_{L,R}\left(-\tfrac{1}{2}a\right) = \psi_{L,R}^I, \tag{E6}$$

$$\lim_{a\to 0}\psi_{L,R}\left(\tfrac{3}{2}a\right) = \lim_{a\to 0}\psi_{L,R}\left(\tfrac{1}{2}a\right) = \psi_{L,R}^{II}, \tag{E7}$$

Solving for ψ_L^I in Eq. (E4) and putting it into Eq. (E5), we have

$$\psi_R^I = \frac{1}{2\alpha\tau}\left(i(\tau^2 - \alpha^2 - \epsilon^2)\psi_L^{II} + (\tau^2 - (\epsilon + i\alpha)^2)\psi_R^{II}\right). \tag{E8}$$

Inserting this expression into Eq. (E4), we arrive at

$$\psi_L^I = \frac{1}{2\alpha\tau}\left((\tau^2 + (\alpha + i\epsilon)^2)\psi_L^{II} - i(\tau^2 - \alpha^2 + \epsilon^2)\psi_R^{II}\right). \tag{E9}$$

We can express these two equations as $\psi^I = T\psi^{II}$, where T is a transfer matrix:

$$\begin{pmatrix}\psi_L^I\\ \psi_R^I\end{pmatrix} = \frac{1}{2\alpha\tau}\begin{pmatrix}\tau^2 + (\alpha + i\epsilon)^2 & -i(\tau^2 - \alpha^2 + \epsilon^2)\\ i(\tau^2 - \alpha^2 - \epsilon^2) & \tau^2 - (\epsilon + i\alpha)^2\end{pmatrix} \times \begin{pmatrix}\psi_L^{II}\\ \psi_R^{II}\end{pmatrix}. \tag{E10}$$

Furthermore, at half filling we have that $\epsilon \xrightarrow[L\to\infty]{} 0$ and the transfer matrix simplifies to

$$T = \frac{1}{2\alpha\tau}\begin{pmatrix}\tau^2 + \alpha^2 & -i(\tau^2 - \alpha^2)\\ i(\tau^2 - \alpha^2) & \tau^2 + \alpha^2\end{pmatrix}. \tag{E11}$$

Note that this can be also written as

$$T = \frac{1}{2\tilde{\tau}}\begin{pmatrix}\tilde{\tau}^2 + 1 & -i(\tilde{\tau}^2 - 1)\\ i(\tilde{\tau}^2 - 1) & \tilde{\tau}^2 + 1\end{pmatrix}, \tag{E12}$$

where $\tilde{\tau} = \frac{\tau}{\alpha}$. Substituting $\tau = e^{-h\gamma}$ and $\alpha = e^{-\frac{h}{2}}$ we have the expression Eq. (25).

APPENDIX F: DETAILS OF THE RG APPLIED TO THE SCS SYSTEM

In this Appendix, we derive the ground state of the Hamiltonian

$$H_N(h,\gamma)_{\text{scs}} = -\frac{1}{2}\sum_{m=1}^{N} J_m c_m^\dagger c_{m+1} + \text{H.c.}, \quad \text{with}$$

$$J_m = \begin{cases} e^{-h(|m-(L+\frac{1}{2})|-\frac{1}{2})} & \text{if } m \neq L, L+1,\\ e^{-h\gamma} & \text{if } m \in \{L, L+1\}.\end{cases} \tag{F1}$$

We use the RG scheme explained in the main text. There are three cases to be considered.

(1) Case $\gamma < 1$. The couplings present a double tie at the center, so that the dominant interaction involves the three central sites, L, $L+1$ and $L+2$. The Dasgupta-Ma prescription Eq. (A2) and the sum rule Eq. (A3) are not valid in this situation. We must perform a first-order perturbation approach to renormalize three fermionic sites into an effective site (see Appendix A of Ref. [22]), leading to a system with $N-2$ sites. The next RG step involves the effective fermion mode created on the previous one and its two nearest neighbours. Iterating this procedure one obtains the GS:

$$|\text{GS}\rangle_{\gamma<1} = \left(g_L^\xi\right)^\dagger \prod_{m=1}^{L-2}\left(f_m^{s_m}\right)^\dagger (g_0^+)^\dagger |0\rangle, \tag{F2}$$

where $s_m = (-1)^m$, $\xi = (-1)^{\frac{L}{2}}$ and

$$g_m^\pm = \frac{1}{\sqrt{2}}(c_{L+1} + b^\pm_{L-2m,L+2(m+1)}), \tag{F3}$$

$$g_L^\pm = \frac{1}{\sqrt{2}}(c_1 + b^\pm_{2,2L}), \tag{F4}$$

$$f_n^\pm = \frac{1}{\sqrt{2}}(b^\pm_{L+1-n,L+1+n} + b^\pm_{L-n,L+2+n}), \tag{F5}$$

with $b^\pm_{i,j}$ defined in Eq. (7).

(2) Case $\gamma = 1$. The system presents a quadruple tie at the center. The five central sites involved are renormalized into an effective site on a system with $N-4$ sites. At this point the situation is equivalent to the $\gamma < 1$ case and further RG steps are the same as the ones discussed in the previous item.

(3) Case $\gamma > 1$. In this situation, the dominant interactions are two nonconsecutive log-couplings 1, which couple respectively the sites $L-1$ and L, and the sites $L+2$ and $L+3$. Although the sum rule (A3) is not valid, the Dasgupta-Ma equation (A2) can be applied sequentially twice, yielding two fermionic excitations with the same energy and parity, $b^+_{L-1,L}$ and $b^+_{L+2,L+3}$, and leading to a effective system whose Hamiltonian is $H_{N-4}(h, 1+\gamma)_{\text{scs}}$. The next decimation step is not univocal.

(i) If $\gamma \in (1, 2)$ the dominant interaction involves the three central sites $L-2$, L and $L+4$ of the original chain and the

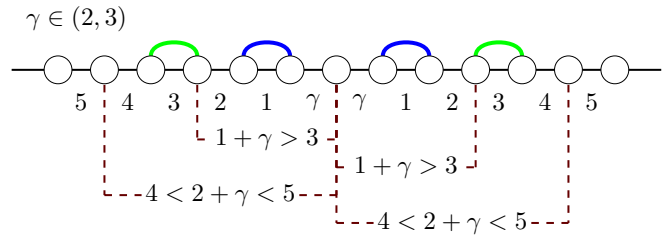

FIG. 15. RG procedure for a system $H_N(h,\gamma)_{\text{scs}}$ with $h \gg 1$ and $\gamma \in (2,3)$. The system admits two Dasgupta-Ma RG steps, above links with log-coupling 1, and after those the renormalized system shows a double tie of lowest log-couplings, with the two central log-couplings equal to $1+\gamma$ (which must be larger than 3). At this moment, we apply the same RG procedure than for $\gamma < 1$.

situation is the same as the one described originally for $\gamma < 1$, with the double tie (1).

(ii) If $\gamma = 2$ there is a quadruple tie, same as (2).

(iii) If $\gamma \in (2, 3)$ the dominant interactions are the two links with log-coupling 3, which is similar to the situation described in item (3). At the end of this step there are two fermionic excitations more, $b^+_{L-3,L-2}$ and $b^+_{L+4,L+5}$, and the Hamiltonian of the decimated system is $H_{N-8}(h, 2+\gamma)_{\text{scs}}$. We show in Fig. 15 this situation.

Note that unless $\gamma > L-1$ the RG flows towards the double tie situation and, if $\gamma \in \mathbb{N}$, the decimated system of the γth step will present a quadruple tie. Hence, the GS is

$$|\text{GS}\rangle_{\gamma>1} = (g^-_L)^\dagger \prod_{k=1}^{L-2(1+\lfloor\gamma\rfloor)} \left(f^{\eta_k}_{k+2\lfloor\gamma\rfloor}\right)^\dagger (g^-_{\lfloor\gamma\rfloor})^\dagger \times \prod_{m=1}^{\lfloor\gamma\rfloor} (b^+_{L-2(m-1),L-2(m-1)-1})^\dagger (b^+_{L+2m,L+2m+1})^\dagger |0\rangle, \tag{F6}$$

where $\lfloor\rfloor$ is the floor function, $\eta_k = (-1)^{k+1}$, $\chi_k = (-1)^{k-\lfloor\gamma\rfloor}$.

[1] L. Amico, R. Fazio, A. Osterloh, and V. Vedral, Entanglement in many-body systems, Rev. Mod. Phys. **80**, 517 (2008).

[2] N. Laflorencie, Quantum entanglement in condensed matter systems, Phys. Rep. **646**, 1 (2016).

[3] M. B. Hastings, Solving gapped Hamiltonians locally, Phys. Rev. B **73**, 085115 (2006).

[4] M. M. Wolf, F. Verstraete, M. B. Hastings, and J. I. Cirac, Area Laws in Quantum Systems: Mutual Information and Correlations, Phys. Rev. Lett. **100**, 070502 (2008).

[5] M. Srednicki, Entropy and Area, Phys. Rev. Lett. **71**, 666 (1993).

[6] J. Eisert, M. Cramer, and M. B. Plenio, Area-laws for the entanglement entropy: a review, Rev. Mod. Phys. **82**, 277 (2010).

[7] C. Holzhey, F. Larsen, and F. Wilczek, Geometric and renormalized entropy in conformal field theory, Nucl. Phys. B **424**, 443 (1994).

[8] G. Vidal, J. I. Latorre, E. Rico, and A. Kitaev, Entanglement in Quantum Critical Phenomena, Phys. Rev. Lett. **90**, 227902 (2003).

[9] P. Calabrese and J. L. Cardy, Entanglement entropy and quantum field theory, J. Stat. Mech. (2004) P06002.

[10] P. Calabrese and J. Cardy, Entanglement entropy and conformal field theory, J. Phys. A **42**, 504005 (2009).

[11] G. Refael and J. E. Moore, Entanglement Entropy of Random Quantum Critical Points in One Dimension, Phys. Rev. Lett. **93**, 260602 (2004).

[12] G. Refael and J. E. Moore, Criticality and entanglement in random quantum systems, J. Phys. A **42**, 504010 (2009).

[13] N. Laflorencie, Scaling of entanglement entropy in the random singlet phase, Phys. Rev. B **72**, 140408(R) (2005).

[14] M. Fagotti, P. Calabrese, and J. E. Moore, Entanglement spectrum of random-singlet quantum critical points, Phys. Rev. B **83**, 045110 (2011).

[15] G. Ramírez, J. Rodríguez-Laguna, and G. Sierra, Entanglement in low-energy states of the random coupling model, JSTAT **2014** (2014) P07003.

[16] P. Ruggiero, V. Alba, and P. Calabrese, The entanglement negativity in random spin chains, Phys. Rev. B **94**, 035152 (2016).

[17] C. Dasgupta and S.-K. Ma, Low-temperature properties of the random Heisenberg antiferromagnetic chain, Phys. Rev. B **22**, 1305 (1980).

[18] D. S. Fisher, Critical behavior of random transverse-field Ising spin chains, Phys. Rev. B **51**, 6411 (1995).

[19] G. Vitagliano, A. Riera, and J. I. Latorre, Volume-law scaling for the entanglement entropy in spin 1/2 chains, New J. Phys. **12**, 113049 (2010).

[20] G. Ramírez, J. Rodríguez-Laguna, and G. Sierra, From conformal to volume-law for the entanglement entropy in exponentially deformed critical spin 1/2 chains, J. Stat. Mech. (2014) P10004.

[21] G. Ramírez, J. Rodríguez-Laguna, and G. Sierra, Entanglement over the rainbow, J. Stat. Mech. (2015) P06002.

[22] N. Samos Sáenz de Buruaga, S. N. Santalla, J. Rodríguez-Laguna, and G. Sierra, Symmetry protected phases in inhomogeneous spin chains, J. Stat. Mech. (2019) 093102.

[23] J. Rodríguez-Laguna, S. N. Santalla, G. Ramírez, and G. Sierra, Entanglement in correlated random spin chains, RNA folding and kinetic roughening, New J. Phys. **18**, 073025 (2016).

[24] V. Alba, S. N. Santalla, P. Ruggiero, J. Rodríguez-Laguna, P. Calabrese, and G. Sierra, Unsual area-law violation in random inhomogeneous systems, J. Stat. Mech. (2019) 023105.

[25] O. Boada, A. Celi, J. I. Latorre, and M. Lewenstein, Dirac equation for cold atoms in artificial curved spacetimes, New J. Phys. **13**, 035002 (2011).

[26] J. Rodríguez-Laguna, L. Tarruell, M. Lewenstein, and A. Celi, Synthetic Unruh effect in cold atoms, Phys. Rev. A **95**, 013627 (2017).

[27] J. Rodríguez-Laguna, J. Dubaîl, G. Ramírez, P. Calabrese, and G. Sierra, More on the rainbow chain: entanglement, space-time geometry and thermal states, J. Phys. A **50**, 164001 (2017).

[28] E. Tonni, J. Rodríguez-Laguna, and G. Sierra, Entanglement hamiltonian and entanglement contour in inhomogeneous 1D critical systems, J. Stat. Mech. (2018) 043105.

[29] I. MacCormack, A. L. Liu, M. Nozaki, and S. Ryu, Holographic duals of inhomogeneous systems: The rainbow chain and the sine-square deformation model, J. Phys. A: Math. Theor. **52** 505401 (2019).

[30] R. N. Alexander, A. Ahmadain, Z. Zhang and I. Klich, Holographic rainbow networks for colorful Motzkin and Fredkin spin chains, Phys. Rev. B **100**, 214430 (2019).

[31] G. C. Levine, Entanglement Entropy in a Boundary Defect Model, Phys. Rev. Lett. **93**, 266402 (2004).

[32] I. Peschel, Entanglement entropy with interface defects, J. Phys. A: Math. Gen. **38**, 4327 (2005).

[33] F. Iglói, Z. Szatmári, and Y.-C. Lin, Entanglement entropy with localized and extended defects, Phys. Rev. B **80**, 024405 (2009).

[34] V. Eisler and I. Peschel, Entanglement in fermionic chains with interface defects, Ann. Phys. (Berlin) **522**, 679 (2010).

[35] W. P. Su, J. R. Schrieffer, and A. J. Heeger, Solitons in Polyacetylene, Phys. Rev. Lett. **42**, 1698 (1979).

[36] A. J. Heeger, S. Kivelson, J. R. Schrieffer, and W.-P. Su, Solitons in conducting polymers, Rev. Mod. Phys. **60**, 781 (1988).

[37] R. Vasseur, A. C. Potter, Yi-Zhuang, and A. W. W. Ludwig, Entanglement transitions from holographic random tensor networks, Phys. Rev. B **100**, 134203 (2019).

[38] I. Peschel, Calculation of reduced density matrices from correlation functions, J. Phys. A: Math. Gen. **36**, L205 (2003).

[39] G. Sierra, The Riemann zeros as energy levels of a Dirac fermion in a potential built from the prime numbers in Rindler spacetime, J. Phys. A: Math. Theor. **47**, 325204 (2014).

[40] M. Abramowitz and I. A. Stegun, *Handbook of Mathematical Functions with Formulas, Graphs, and Mathematical Tables*, Applied Mathematics Series - 49 (US Department of Commerce, National Bureau of Standards, 1948), p. 1004

[41] B.-Q. Jin and V. E. Korepin, Quantum spin chain, Toeplitz determinants and the Fisher–Hartwig conjecture, J. Stat. Phys. **116**, 79 (2004).

[42] J. Cardy and E. Tonni, Entanglement Hamiltonians in two-dimensional conformal field theory, J. Stat. Mech. (2016) 123103.

[43] H. Li and F. D. M. Haldane, Entanglement Spectrum as a Generalization of Entanglement Entropy: Identification of Topological Order in Non-Abelian Fractional Quantum Hall Effect States, Phys. Rev. Lett. **101**, 010504 (2008).

[44] A. M. Läuchli, Operator content of real-space entanglement spectra at conformal critical points, arXiv:1303.0741v1

[45] Y. Chen and G. Vidal, Entanglement contour, J. Stat. Mech. (2014) P10011.

[46] A. Coser, C. de Nobili, E. Tonni, A contour for the entanglement entropies in harmonic lattices, J. Phys. A: Math. Theor. **50**, 314001 (2017).

[47] S. Singha Roy, S. N. Santalla, J. Rodríguez-Laguna, and G. Sierra, Entanglement as geometry and flow, arXiv:1906.05146.

[48] T. Kennedy and H. Tasaki, Hidden symmetry breaking and the haldane phase in s = 1 quantum spin chains, Commun. Math. Phys. **147**, 431 (1992).

[49] A. Altland and M. R. Zirnbauer, Nonstandard symmetry classes in mesoscopic normal-superconducting hybrid structures, Phys. Rev. B **55**, 1142 (1997).

[50] F. Pollmann, A. M. Turner, E. Berg, and M. Oshikawa, Entanglement spectrum of a topological phase in one dimension, Phys. Rev. B **81**, 064439 (2010).

[51] L. Fidkowski and A. Kitaev, Topological phases of fermions in one dimension, Phys. Rev. B **83**, 075103 (2011).

[52] A. M. Turner, F. Pollmann and E. Berg, Topological phases of one-dimensional fermions: An entanglement point of view, Phys. Rev. B **83**, 075102 (2011).

[53] X. Chen, Z.-C. Gu and X.-G. Wen, Classification of Gapped Symmetric Phases in 1D Spin Systems, Phys. Rev. B **83**, 035107 (2011).

[54] X. Chen, Z.-C. Gu and X.-G. Wen, Complete classification of 1D gapped quantum phases in interacting spin systems, Phys. Rev. B **84**, 235128 (2011).

[55] F. Pollmann, E. Berg, A. M. Turner, and M. Oshikawa, Symmetry protection of topological order in one-dimensional quantum spin systems, Phys. Rev. B **85**, 075125 (2012).